Title: Human deep sleep facilitates faster cerebrospinal fluid dynamics linked to brain oscillations for sleep homeostasis and memory

Authors: Makoto Uji[1], Xuemei Li[1], An Saotome[1,2], Ryosuke Katsumata[1,3], R. Allen Waggoner[1], Chisato Suzuki[1], Kenichi Ueno[1], Sayaka Aritake[1,2], Masako Tamaki[1,4*]

Affiliations:

[1] RIKEN Center for Brain Science, Saitama, Japan

[2] Saitama Prefectural University, Saitama, Japan

[3] Chiba University, Chiba, Japan

[4] RIKEN Cluster for Pioneering Research, Saitama, Japan

*Correspondence to: Masako Tamaki (masako.tamaki@riken.jp)

Abstract (up to 150 words):

While cerebrospinal fluid (CSF) dynamics during sleep have been implicated in metabolic waste reduction in animals, how CSF dynamics are driven in the human brain remains elusive. Here, by leveraging a simultaneous sparse-fMRI and polysomnography method designed specifically for acquiring deep stable sleep data, we present the first evidence of deep sleep-specific faster CSF dynamics in healthy young human participants. Slow waves and sleep spindles during slow-wave sleep and rapid eye movements and sawtooth waves during rapid eye movement (REM) sleep induce frequent low-amplitude CSF fluctuations, contributing to faster CSF dynamics during deep sleep. In contrast, arousal-related brain activities during light sleep produced infrequent large CSF changes. Furthermore, these brain oscillations during light and deep sleep recruited essentially

different brain networks, with deep sleep emphasizing memory and homeostatic circuits. Thus, human deep sleep has a unique way of enabling faster CSF dynamics that are distinctive from arousal mechanisms.

(148 / 150 words)

Main Text:

Sleep is undeniably crucial for the maintenance of healthy brain functions[1–3]. Poor sleep results in a wide variety of health problems, including neurodegenerative diseases such as Alzheimer's disease[3,4]. However, how sleep maintains human brain functions has remained one of the biggest mysteries in neuroscience, medicine, and daily life.

Cerebrospinal fluid (CSF) dynamics during sleep have recently been proposed as one of the essential mechanisms for supporting brain functions. Research on animal models has suggested that brain metabolite waste is reduced specifically during sleep[5]. This process relies on CSF dynamics to wash out metabolic waste from the brain[6,7]. In rodents, CSF dynamics reach maximum levels during deep nonrapid-eye-movement (NREM) sleep or slow-wave sleep[5]. Empirical measurements of CSF dynamics during human sleep are scarce, but CSF dynamics during sleep may also play a similar role in humans. One study has shown that CSF tracer molecules are spread out and then cleared from the brain during sleep, whereas sleep deprivation impairs these processes[6]. Furthermore, sleep quality was also correlated with the amount of clearance[8].

The current dominant view of CSF regulation during human sleep is the ascending arousal model for CSF dynamics[9,10]. By measuring functional MRI (fMRI) during light NREM sleep, which comprises the N1 and N2 sleep stages, the slow frequency component (~0.05 Hz) in the CSF signals was found to be stronger during sleep than during wakefulness[9–11]. This slow frequency component is likely to be produced by K-complexes during light NREM sleep[9], which are known to be associated with arousal[12–15]. However, the type of sleep that has a strong reciprocal relationship with brain health is deep stable sleep, which includes slow-wave sleep and rapid eye movement (REM) sleep. Aging and sleep disorders increase arousal, resulting in decreased deep sleep[16,17]. Along with evidence showing the roles of slow-wave sleep and REM sleep in memory[18–

[23], deep sleep stages should play a critical role in both maintaining and facilitating brain functions. Moreover, the ascending arousal model for CSF dynamics lacks an explanation as to how arousal can solely regulate the CSF flow when arousal mechanisms are largely suppressed during deep sleep[24].

Alternatively, we propose that sleep brain oscillations and events during deep sleep[25–27] provide a plausible mechanism for CSF flow modulations[28]. Since brain oscillations and events, including slow waves and sleep spindles, continuously occur during deep sleep[29], if these brain events indeed modulate the fluid flow, the CSF signals should oscillate much faster than those during wakefulness or light sleep. These rationales led to our hypothesis that human deep sleep plays a major and specific role in accelerating CSF dynamics, which is tightly linked to sleep brain oscillations and events. We further hypothesize that deep sleep mechanisms are distinct from arousal mechanisms.

Importantly, no study thus far has succeeded in measuring CSF signals during slow-wave sleep or rapid-eye movement (REM) sleep in humans. This is because measuring brain activity during deep human sleep inside an MRI scanner has been extremely challenging due to the large, continuous acoustic noise produced during MRI scans. The acoustic noise in MRI scans is known to cause frequent arousals and prolonged wakefulness, inhibiting participants from reaching deeper sleep even after sleep deprivation[10,30,31]. This issue has prevented previous research from measuring CSF dynamics during slow-wave sleep or REM sleep in humans.

The present study overcame this technical difficulty and successfully measured fMRI signals from the lateral ventricles (CSF signals) during slow-wave sleep and REM sleep in healthy young participants. We developed a minimally disturbing cutting-edge fMRI sequence measured simultaneously with polysomnography (PSG), in which a quiet period was inserted between MRI

image acquisitions, allowing participants to sleep deeper. We report that CSF signals fluctuate significantly faster during slow-wave sleep and REM sleep than during light sleep, facilitated by abundant sleep brain oscillations and events, including slow waves, sleep spindles, rapid eye movements, and sawtooth waves. We demonstrate for the first time that sleep brain oscillations and neural events during deep stable sleep can modulate CSF dynamics distinct from the arousal mechanisms in human participants, indicating a fundamental property of deep sleep for the maintenance of brain functions. The present study therefore offers a clue as to why deep and stable sleep matters for the human brain.

Results

Leveraging simultaneous sparse fMRI and polysomnography (PSG) measurements designed for measuring stable sleep data (**Fig. 1a**; see ***Experimental design*** and ***MRI acquisition*** in **Methods**), we acquired a total of 50 sleep datasets from twenty-five young healthy participants (mean 23.6 ± 4.8 years old, 15 female). This sparse fMRI protocol was inspired by previous studies that successfully acquired slow-wave sleep and REM sleep data using magnetic resonance spectroscopy (MRS), where the duration of MRI signal acquisition was approximately 1 s, separated by quiet periods[23,32]. In contrast to regular fMRI sequences, which produce continuous sharp acoustic noise that is known to prevent participants from sleeping deeply, the current sparse fMRI sequence has a 2.1 s quiet period between MRI image acquisitions (=900 ms), emulating the MRS sequence. Using this protocol, the present study succeeded in collecting deep sleep data. The average sleep duration was 69.6 ± 2.9 min (*mean* ± *SE*), including 18–30 sessions with slow-wave sleep and/or REM sleep data (**Table 1**). The fMRI data were denoised using cardiac and respiration

signals[33,34]. The CSF signals were extracted from each participant's lateral ventricles (**Fig. 1b & c**). Any epochs containing arousals or motion artifacts were removed from further analyses.

Slow-wave sleep and REM sleep induce faster CSF components

Slow-wave sleep is characterized by ample slow waves and sleep spindles, whereas REM sleep involves rapid eye movements and sawtooth waves[29,35]. If CSF signals are modulated by brain oscillations and neural events independent of arousal, CSF signals would fluctuate *faster* during slow-wave sleep than during light sleep, considering the abundance of these oscillations during deep sleep. To specifically examine the frequency characteristics of the CSF dynamics, we examined the periodic oscillation components of CSF signals across different sleep depths, identifying three different frequency components: slow (< 0.06 Hz), fast (0.06–0.12 Hz) and very fast (>0.12 Hz) components (see ***Power spectrum analysis of fMRI data*** in **Methods**).

Our results revealed that the fast component power in the CSF signals was significantly greater during slow-wave sleep than during wakefulness or light NREM sleep (**Fig. 1d & e**, blue; **Supplementary Fig. S1b & d**). In contrast, the slow component power in the CSF signals was significantly greater during light NREM sleep than during wakefulness or slow-wave sleep (**Fig. 1d & e**, green; **Supplementary Fig. S1a & d**). CSF dynamics during REM sleep were characterized by a mixture of slow and very fast components (**Fig. 1d & e**, red; **Supplementary Fig. S1e & f**). Similar to light NREM sleep, the slow component power was significantly greater during REM sleep than during slow-wave sleep (**Supplementary Fig. S1f**) or wakefulness (**Supplementary Fig. S1c**). However, the power of the very fast component was significantly greater during REM sleep than during light NREM sleep (**Fig. 1d & e**; **Supplementary Fig. S1e**). These findings demonstrate that both slow-wave sleep and REM sleep are indeed characterized by

124 higher frequency CSF dynamics than light sleep (see **Supplementary Fig. S2** for the relationship
125 between CSF signals and whole gray matter (GM) signals).

126 Previous reports have extracted fMRI signals from the fourth ventricle[9,11,36] to investigate
127 the CSF signal changes potentially reflecting inflow during light sleep and wakefulness. We next
128 asked whether the sleep depth-dependent changes in the frequency profiles could be found
129 specifically in the lateral ventricles or could be found elsewhere in the ventricles. To test this, we
130 examined CSF signals in the fourth ventricle (**Supplementary Note**, **Supplementary Figs. S3–**
131 **S5**). As in the lateral ventricles, slow-wave sleep was dominated by the fast frequency component
132 (**Supplementary Fig. S4b & d**, **Fig. S5b & d**; all $Ps < 0.05$), whereas light NREM sleep was
133 characterized by the slow frequency component (**Supplementary Fig. S4a & d**, **Fig. S5a & d**; all
134 $Ps < 0.05$). Thus, regardless of the ventricles analyzed, deep sleep is characterized by greater high-
135 frequency power in the CSF signal.

136

137 **Slow waves and sleep spindles facilitate CSF fluctuations during slow-wave sleep**

138 We next directly tested whether the higher-frequency CSF dynamics during slow-wave
139 sleep are induced by brain oscillations, such as slow waves and sleep spindles, independent of
140 arousal mechanisms. To test this, EEG signals recorded simultaneously with fMRI data had
141 artifacts removed, and then slow waves and sleep spindles were detected from the EEG signals
142 during light NREM and slow-wave sleep (see ***Sleep event detection*** and ***fMRI time course***
143 ***analysis*** in **Methods**, **Fig. 2a**). The CSF signal changes were measured for each event. If sleep
144 brain oscillations modulate CSF signals, significant changes in the CSF signals would be observed
145 after the onset of oscillations. We first confirmed that slow waves occurred significantly more
146 frequently during slow-wave sleep than during light NREM sleep (**Fig. 2b**; mean intervals between

events, light NREM sleep, 73.9 ± 13.05 s; slow-wave sleep, 14.8 ± 3.52 s, *mean* ± *SE*; two-tailed paired *t*-test, $P = 0.012$), whereas spindles occurred more frequently during light NREM sleep than during slow-wave sleep (**Fig. 2b**; mean intervals between events, light NREM sleep, 5.3 ± 0.29 s; slow-wave sleep, 6.8 ± 0.41 s, two-tailed paired *t*-test, $P = 0.0002$).

Importantly, CSF signal changes induced by brain oscillations exhibit different characteristics depending on the depth of sleep. During light NREM sleep, in addition to sleep spindles that induced significant CSF signal changes at 6 s after onset (**Fig. 2c**, dark green), slow waves induced a large CSF signal peak at 8 s after onset (**Fig. 2c**, light green). In contrast, during slow-wave sleep, slow waves triggered CSF signal changes peaking at 5.5 s **(Fig. 2d**, light blue), which was significantly smaller in amplitude (**Fig. 2e**, two-tailed paired *t*-test, $P = 0.00003$) and shorter in latency (**Fig. 2f**, two-tailed paired *t*-test, $P = 0.00003$) than light NREM sleep, indicating faster and milder CSF circulation in association with ample brain oscillations during slow-wave sleep. During slow-wave sleep, sleep spindles again induced CSF signal changes at 4 s after their onset, which lasted for approximately 10 s (**Fig. 2d**, dark blue). These findings demonstrate that CSF signal changes are indeed correlated with brain oscillations during sleep. See **Supplementary Fig. S6** for the GM signal changes and their relationship to the CSF signals.

To further confirm the tight relationship between the CSF signal changes and sleep brain oscillations, we conducted an inverse analysis; we investigated the EEG topographical changes based on CSF signal positive peak events (see ***CSF peak locked EEG topography analysis*** in **Methods**). The segmented EEG data were averaged for each sleep stage (**Supplementary Fig. S7**). The EEG topographic map indicated a negative peak centered around the frontal region, resembling a topography of K-complexes, which peaked 8 s *before* the CSF positive peak events during light NREM sleep (note that slow waves during light NREM sleep were followed by a CSF

peak 8s *after* the onset of slow wave events, **Fig. 2c**). During slow-wave sleep, a negative peak spread through the midline of frontal to parietal regions resembling those found typically in slow waves[37] which peaked around 5 s *before* the CSF positive peak events during slow-wave sleep (note that slow waves during slow-wave sleep were followed by a CSF peak 5.5s *after* the onset of slow wave events, **Fig. 2d**). These inverse analyses further confirmed that sleep brain oscillations and CSF signal fluctuations are tightly linked.

Rapid eye movements and sawtooth waves during REM sleep modulate CSF fluctuations

Do brain oscillations modulate CSF dynamics only during NREM sleep? Rapid eye movements and sawtooth waves during REM sleep have been associated with memory processing and conscious experiences[27,38,39]. Thus, if neural activities during REM sleep, not limited to NREM sleep events, contribute to CSF signal changes, CSF signals should show significant changes that are time-locked to these events. To this end, we detected typical REM sleep events, such as rapid eye movements and sawtooth waves observed during REM sleep (**Fig. 3a**; ***Sleep event detection*** in **Methods**). We combined all of the REM sleep events together since the number of events was limited (**Fig. 3b**). We found that REM sleep events increased the signal fluctuations 30 s after the onset of the events (**Fig. 3c**; see **Supplementary Fig. S8a–b** for the results for each event). In contrast to NREM sleep events, REM sleep events took a longer time to induce a smaller CSF signal fluctuation (**Fig. 3c**). We next tested whether global brain activation occurs prior to the CSF peaks, similar to NREM sleep. We found that REM sleep events also induced a GM signal increase at 20 s after onset (**Fig. 3d**; **Supplementary Fig. S8c–d**), approximately 10 s before the CSF peak. However, REM sleep events showed a significant positive, not negative, correlation between the CSF and GM signals (**Fig. 3e**, $r = 0.31$ at lag -6.1 s, $P < 1e\text{-}10$), suggesting different mechanisms

193 for CSF and GM coupling between NREM and REM sleep (see also **Supplementary Fig. S6c &**
194 **d** for CSF and GM coupling during NREM sleep).
195
196 **Different contributions of sleep brain oscillations and ascending arousal mechanisms to CSF**
197 **dynamics**
198 Thus far, our results indicate that brain oscillations and neural events during deep sleep
199 modulate CSF dynamics. Could these changes be explained solely by the ascending arousal
200 mechanisms as previous studies[10,30] have indicated? If so, similar changes in the CSF signals could
201 be induced by sleep-related brain oscillations and arousal. To investigate whether the contributions
202 of sleep-related brain oscillations to CSF fluctuations are based on arousal mechanisms, we
203 examined arousal-induced CSF signal changes and directly compared them with sleep-related
204 brain oscillation-induced CSF signal changes. Arousal events in the EEG signals were detected by
205 sleep experts in accordance with the standard criteria[35]. The arousal events were defined as an
206 abrupt shift in EEG frequency, which was clearly visible in the EEG signals (**Fig. 4a**; ***Sleep event***
207 ***detection*** in **Methods**). The CSF and GM signals were subsequently segmented on the basis of
208 each arousal onset.
209 The arousals occurred more often during light NREM sleep (21.2 ± 1.9) than during slow-
210 wave sleep (0.3 ± 0.1; **Fig. 4b**; two-tailed paired *t*-test, P = 1.8225e-10) or REM sleep (0.9 ± 0.2;
211 **Fig. 4b**; two-tailed paired *t*-test, P = 4.1543e-08). These findings confirm that deep sleep is the
212 least prone to arousals. Next, CSF signal changes time-locked to arousal events were measured.
213 The average CSF signals increased 8 s after the onset of the arousal events and then returned to
214 baseline 20 s after onset (**Fig. 4c**, black). Arousal-related CSF and GM signal changes were similar
215 across sleep stages (**Fig. 4c, d**), with the exception that the CSF signal changes to arousals were

216 barely visible during slow-wave sleep (**Fig. 4c**). Notably, the CSF and GM signal changes caused
217 by arousals and slow waves during light NREM sleep had similar signal properties (**Fig. 4e, f**).
218 The latency to reach the peak CSF signal was approximately 8 s (**Fig. 4e, h**), and CSF signal
219 changes were followed by a large GM undershoot (**Fig. 4f**). In contrast, slow waves during slow-
220 wave sleep induced a shorter latency (**Fig. 4e, h**; P = 2.0568e-07) and smaller amplitude changes
221 (**Fig. 4e & g**; P = 2.0568e-07) in the CSF signals as compared to the arousals (see **Supplementary**
222 **Fig. S9** for each comparison). One may wonder whether the differences in the signal properties
223 between arousals and slow waves are simply due to the frequencies of the events, as a larger
224 number of events may induce larger accumulative changes. However, since the total number of
225 slow waves during slow-wave sleep (77.8 ± 21.8) was significantly greater than the total number
226 of arousals (22.7 ± 1.9; P = 0.0175), this is unlikely.

227 These findings consistently indicate that arousals and slow waves during light sleep induce
228 slow and large CSF fluctuations, whereas slow waves during slow-wave sleep induce fast yet small
229 CSF signal changes, suggesting that sleep depth-dependent brain oscillations and ascending
230 arousal circuits contribute differently to CSF fluctuations.

231

232 **CSF dynamics associated with respiration, cardiac rhythms, and head motions**

233 Since previous studies demonstrated tight coupling among respiration, cardiac pulses, and
234 CSF dynamics[10,36,40], we performed additional control analyses and confirmed that none of the
235 respiratory or cardiac rhythms were likely to have caused the differences in the CSF dynamics
236 among sleep stages and brain oscillations.

237 First, the intervals of the events were longer during the deep sleep stages than during the
238 light sleep stages. Cardiac cycles were significantly longer during slow-wave sleep or REM sleep

than during wakefulness (slow-wave sleep vs. wakefulness: P = 7.85e-07; REM sleep vs. wakefulness: P = 5.31e-04; **Supplementary Fig. S10a**). There was no significant difference in respiratory cycles across different sleep depths (**Supplementary Fig. S10b**). Second, the periodic frequency changes across different sleep depths were not produced by denoising processes during the fMRI preprocessing. To this end, we investigated the periodic component of CSF signals across different sleep depths without denoising processes of respiration and cardiac pulses following previous studies[33,34]. The key findings in the periodic frequency changes remained regardless of the existence of respiration and cardiac cycles in the fMRI signals (**Supplementary Figs. S11–13**). Third, although a gradual increase occurred in the CSF signals after the respiration and cardiac pulses, these changes were significantly smaller than the CSF signal changes that occurred after brain oscillations (**Supplementary Fig. S14**). Fourth, the cardiac and respirations had higher frequency signals (cardiac: around 1Hz; respiration: around 0.3Hz; **Supplementary Fig. S15** and **Fig. 1d**) that did not overlap with the frequency range induced by sleep brain oscillations (fast: 0.06–0.12 Hz, very fast: 0.12–0.15 Hz; **Fig. 1d**). Thus, these physiological signals are not the main causes of the faster oscillating CSF signals found during slow-wave sleep and REM sleep.

Additionally, one may wonder whether our findings were caused by confounders such as head motion. We further performed a control analysis to investigate the effects of head motion in our current dataset. To this end, we examined differences in the distance of head motion during fMRI scans across different sleep depths. We found that head motion during slow-wave sleep (0.021 ± 0.002 mm/volume) was significantly smaller than that during light NREM (0.027 ± 0.002 mm/volume, P=0.0056) or REM sleep (0.025 ± 0.002 mm/volume, P=0.0057; **Supplementary Fig. S16**). These findings show that deep sleep is the least prone to head motions; thus, the effect of head motion, if any, would have been minimal during deep sleep compared with light sleep.

Sleep-depth-dependent and arousal-associated changes in the brain network

Because brain oscillations during slow-wave sleep are involved in plasticity and homeostatic regulation[41–43], while K-complexes during light sleep involve arousal mechanisms[12–15], we next asked whether the different modulations of CSF and GM signals found during light sleep, deep sleep, and arousals (**Fig. 1d & e**, **Fig. 2c–f**, **Fig. 4e–h**) were, in fact, due to the differences in brain circuits involved during different depths of sleep. To this end, we applied a generalized linear model (GLM) analysis on the fMRI signals to each event.

We found that different cortical networks were recruited depending on the depth of sleep (**Fig. 5**, **Supplementary Tables S1–7**). The prefrontal and hippocampal regions, striatum, and amygdala were more strongly recruited to slow waves during slow-wave sleep than during light NREM sleep (**Fig. 5**, **Supplementary Table S2**), whereas sensorimotor areas, including the parietal and visual cortices and cerebellum, were more strongly activated with slow waves during light NREM sleep than during slow-wave sleep (**Fig. 5**, **Supplementary Table S1**). These findings indicate that different cortical processing underlies slow waves during light NREM vs. slow-wave sleep. Additionally, we found that more localized cortical brain regions were recruited to sleep spindles during slow-wave sleep than during light NREM sleep (**Supplementary Tables S5 & S6**). REM sleep events activated brain regions, including visual areas, the thalamus, the hippocampus, the striatum, and the amygdala (**Fig. 5, Supplementary Tables S3 & S7**). In contrast to slow-wave sleep or REM sleep, arousals involved whole-brain activations not localized to any regions (**Fig. 5**, **Supplementary Table S4**). Taken together, these results demonstrate that brain oscillations involved in regulating CSF dynamics recruit essentially different networks depending on the depth of sleep.

Discussion

The present results robustly indicate that deep human sleep has a unique way of modulating CSF dynamics, as indicated in **Table 2**. The frequency of CSF signals becomes faster during deep sleep than during wakefulness or light sleep. We further revealed that brain oscillations are the sources of these distinct frequency profiles. Slow waves and sleep spindles during slow-wave sleep induce faster changes in CSF fluctuations. Neural events during REM sleep, such as rapid eye movements and sawtooth waves, also accelerate CSF dynamics. In contrast, arousals and brain oscillations during light sleep induce infrequent, sharp CSF changes. We showed that different brain networks are activated by brain oscillations or events during different depths of sleep. Deep sleep recruits brain regions involved in memory and homeostatic regulation, whereas light sleep and arousal recruit whole-brain activation, including the sensory-motor network.

The present study demonstrated that at least two different processes are involved in regulating CSF dynamics in human sleep. The first process is prominent during light sleep when arousals and arousal-related brain activities take the lead in modulating CSF oscillations. The second process is facilitated specifically during deep stable sleep when arousals are largely suppressed. However, during deep sleep, CSF oscillations are enhanced by spontaneous brain oscillations and neural events, such as slow waves, sleep spindles, and REM sleep events. Since sleep events occur more often than arousals during deep sleep, it is highly likely that sleep events, not arousals, are the major contributors to CSF oscillations during deep sleep. We further propose that these two processes are supported by entirely distinctive mechanisms, as shown in **Fig. 6**. The process during light NREM sleep is based on ascending arousal mechanisms ("arousal-based mechanism"), in which transient increases in brain activity increase CSF oscillations by arousing

308 stimuli to subcortical regions. Arousals occur frequently during light NREM sleep, as we have
309 shown (**Fig. 4b**) and as reported previously[44]. It is also well documented that a particular type of
310 slow wave that dominates light NREM sleep, known as K-complexes, recruits arousal
311 mechanisms[9,12,13]. Another process that we propose here for the first time functions *specifically*
312 during deep sleep ("deep sleep-based mechanism"), which is tightly linked to sleep brain
313 oscillations to drive the CSF oscillations. This deep-sleep mechanism works continuously,
314 producing faster CSF oscillations by tightly interacting with sleep-related brain oscillations. In
315 contrast to the arousal mechanism that induces sharp and transient CSF peaks, the deep-sleep
316 mechanism induces low-amplitude oscillations, potentially causing minimal load to the vascular
317 system while enabling continuous faster oscillations.

318 The higher frequency of CSF oscillations during slow-wave sleep found in the present
319 study might be related to the metabolic waste clearance function suggested in animals[5]. We found
320 that slow waves are among the main oscillations that produce faster CSF circulation during deep
321 sleep. Importantly, slow waves during slow-wave sleep are tightly regulated by homeostatic sleep
322 needs[41]. Given the suggested relationship between prolonged wakefulness or increased brain usage
323 and the accumulation of metabolic waste[6], faster CSF circulation induced by increased slow waves
324 due to increased homeostatic sleep might work well for clearing waste products. Investigating how
325 higher-frequency CSF oscillations during deep sleep contribute to metabolic waste clearance is
326 important in future research.

327 Another key finding in the present study is the contribution of sleep spindles to CSF
328 dynamics. First, we found that sleep spindles facilitate CSF oscillations during sleep. Second, sleep
329 spindles during slow-wave sleep are followed by activations in the brain networks involved in
330 episodic and motor learning (e.g., the hippocampus and striatum). Sleep spindles are known to

331 facilitate episodic and motor learning through plastic changes in cortical and subcortical regions[45–
332 47]. Thus, it is possible that CSF oscillations are coupled not only to sleep homeostasis but also to
333 plasticity processes, where sleep spindles might play a major role.

334 To the best of our knowledge, this is the first study in humans to reveal the modulations of
335 CSF signals by brain activity during REM sleep. We found that REM sleep events, including rapid
336 eye movements and sawtooth waves, the chief events of human REM sleep, enhance CSF signals.
337 While we found faster CSF dynamics during REM sleep as well as during slow-wave sleep, the
338 roles of CSF oscillations might differ. First, we found that not only the very fast component (>
339 0.12 Hz) but also the slow component (< 0.06 Hz) was present in the CSF frequency profiles during
340 REM sleep. Second, the latency to the CSF peak was much longer during REM sleep than during
341 slow-wave sleep. Third, the CSF peak did not accompany the GM undershoot during REM sleep.
342 Interestingly, CSF flows are reduced in pigeons[48] and are predicted to be reduced in rodents[49]. Our
343 results suggest that the CSF dynamics found in the present study are unique to humans, whose
344 REM sleep is more consolidated than that of avians or rodents. How REM sleep regulates CSF
345 oscillations needs to be further investigated. In addition to the rapid eye movements and sawtooth
346 waves we analyzed in this study, theta and alpha activities can be observed via EEG, and muscle
347 twitches occur intermittently during REM sleep, which were not examined here. Although it is
348 widely known that REM sleep data are very difficult to acquire both in humans and in
349 animals[31,48,50], the methodological advancements introduced in the present study (simultaneous
350 sparse fMRI and PSG technique) could facilitate investigations into REM sleep.

351 One may wonder whether cardiac and respiratory rhythms cause differences in the CSF
352 peaks during different sleep stages and brain oscillations since CSF signals are known to be
353 coupled to cardiac and respiratory rhythms[36,51,52]. However, these signals are unlikely to be the

354 sources of the differences in the CSF signal changes among sleep stages and brain oscillations
355 found in the present study for the following three reasons. First, the intervals of the cardiac signals
356 were significantly longer during slow-wave sleep or REM sleep than during wakefulness. There
357 was no significant difference in the respiratory signals across different sleep depths. If these factors
358 contribute to changes in the CSF signal, the CSF signals should be slower during deep sleep than
359 during light sleep. Thus, these rhythms are not in accordance with the significantly faster CSF
360 signals found during slow-wave sleep and REM sleep. Second, we investigated the effects of
361 respiration and cardiac pulses in fMRI signals on the periodic frequency changes in CSF signals.
362 The key findings of the periodic frequency changes in the CSF signals remained regardless of the
363 existence of respiration and cardiac pulses in the fMRI signals. Third, previous studies have
364 indicated that cardiac- and respiration-driven CSF signal changes occur 0.45–1.58 s after the
365 events[36]. However, CSF signal changes caused by slow waves were in the range of 5.5–8 s after
366 the events, much later than the cardiac and respiration-driven changes that might have occurred.
367 Additionally, we investigated the CSF signal changes after respiration and cardiac pulses. We
368 found that respiration- and cardiac-driven signal changes were significantly smaller than sleep-
369 related brain oscillations and arousals. Thus, the CSF peaks caused by cardiac and respiratory
370 rhythms, if any, should not overlap with the CSF peaks caused by brain oscillations.

371 The present study at least partially clarifies why and how deep stable sleep matters for
372 healthy human cognitive functions. Sleep disturbances are a major issue worldwide and are
373 associated with various health-related issues, including cognitive impairments, neurodegenerative
374 diseases and aging[16,53–55]. Importantly, the most striking change found in these cases is the
375 reduction in deep stable sleep. In other words, light NREM sleep most likely remains regardless
376 of the severity of the disorder. Along with evidence showing a strong relationship between the

377 stages of sleep, CSF dynamics, and metabolite clearance[5,6,8,56], dysfunctions in deep sleep may
378 have severe impacts on cognitive functions at least partially via altered CSF flows.

379 Although the present study did not directly measure the underlying mechanisms of the tight
380 link between sleep brain oscillations and the CSF dynamics, one of the likely mechanisms involves
381 vascular dynamics (i.e., vasomotion, vasoconstriction, vasodilation)[9,28,49]. The vascular dynamics
382 may change the size of the perivascular spaces of the penetrating arterioles where the CSF circulate
383 throughout the brain[6,28,49]. Since neural activity, vascular dynamics, and CSF dynamics interact
384 with each other[9,28,49], synchronous neural activities, such as slow waves, sleep spindles, and
385 various REM-sleep events may trigger vasomotion, which may create sufficient spaces for CSF to
386 be circulated[9,28,49]. Based on the present findings, which clearly showed that deep sleep involves
387 faster CSF signal changes, these underlying processes may be more pronounced during deep stable
388 sleep than during light sleep or wakefulness. These further suggest that deep sleep has a specific
389 role in maintaining the tight physiological and neural balance and that light sleep may not be able
390 to compensate for the loss of deep sleep caused by sleep restrictions, aging, or diseases.

391 The following four points need to be addressed in future research. First, our data were
392 obtained from midafternoon naps. Thus, what happens during nightly sleep when sleep needs are
393 greater is unclear. As the duration of slow-wave sleep is the longest and the number of slow waves
394 is the maximum during the first half of nightly sleep[35], it is possible that CSF oscillations are much
395 greater. REM sleep, in contrast, is longest during the early morning, and REM density is greater[35].
396 Thus, REM-related CSF dynamics could benefit from early morning studies. Second, our data are
397 restricted to approximately 1.5 hours, corresponding to the first sleep cycle. Thus, how CSF
398 dynamics change over multiple sleep cycles is unclear. Third, since the present study did not
399 directly measure the amount of metabolite waste or investigate the causal relationship between

CSF and metabolites, how higher-frequency CSF oscillations during deep sleep contribute to waste clearance needs to be clarified in future research. Fourth, the TR in the present study was longer (3 s) than conventionally used (1~2 s) to prioritize the acquisition of deep stable sleep data. Thus, it was not ideal to measure the CSF signal changes driven by the cardiac and respiratory rhythms. Future research is necessary to investigate how physiological rhythms are in accord with CSF signals during deep sleep.

Taken together, the results of the present study clearly reveal the existence of deep sleep-based CSF dynamics, which are regulated by sleep-brain oscillations and events, during slow-wave sleep and REM sleep. These deep sleep-based CSF dynamics are distinct from the arousal-based CSF dynamics previously suggested for the following reasons. First, the frequency components are different between deep and light sleep. Second, the latency and amplitude characteristics are different. Third, the relationships with whole GM signals are different. Fourth, the brain networks induced by sleep brain oscillations during light vs. deep sleep and by arousals are different. While the causal relationship between CSF signals during sleep and brain functions is unclear, the present study collectively suggests that deep sleep-based CSF dynamics are the key to understanding how healthy brain functions are maintained through sleep in humans.

Methods

Participants

Twenty-five young healthy participants (mean age of 23.6 ± 4.8 years, 15 female) participated in this study. All of the participants provided written informed consent for their participation prior to the start of the study. This study was approved by the institutional review board at RIKEN.

Screening process for eligibility

Before consent was obtained, the screening process for eligibility took place to confirm the following aspects. First, the participants were between 18 and 35 years old. Second, on the basis of a self-report questionnaire[23], anyone who had neurological or psychiatric conditions (e.g., epilepsy, migraine, stroke, chronic pain, major depression, anxiety disorder, psychotic disorder), was currently using medication, or was suspected of having a sleep disorder (including insomnia, sleep apnea syndrome, hypersomnolence, restless legs syndrome, parasomnias) was not eligible to participate. Third, participants who had an irregular sleep schedule, i.e., those whose sleep/wake time differed by more than 2 hours between weekdays and weekends, were not eligible. We also ensured that the subjects had not taken a trip to a different time zone during the last six months prior to the experiment. Participants who worked night shifts or who had a habit of taking a nap were not eligible for this study. Fourth, a Pittsburgh Sleep Quality Index (PSQI) was used to assess sleep quality and disturbances over a one-month time interval before the experiments, and a PSQI score within 5 was used as an inclusion criteria[57]. Fifth, those who failed to complete an MRI safety questionnaire (i.e., claustrophobic, pregnant, having metallic objects in the body, such as vascular clips, prosthetic valves, metal prostheses, metal fragments, pacemakers, or dental braces) were not eligible for this study.

440

441 ***Experimental design***

442 All eligible subjects participated in two sleep sessions approximately one week apart. The
443 participants first answered a questionnaire to report their bedtime, wake-up time, and duration of
444 sleep the night before. They also answered the Stanford Sleepiness Scale (SSS) rating[58], which
445 ranges from 1 (feeling active, vital, alert, or wide awake) to 7 (no longer fighting sleep, sleep onset
446 soon; having dream-like thoughts). The subjects were asked to choose the scale rating that
447 described their state of sleepiness. Then, the electrodes for PSG were attached, which took
448 approximately one hour (see the PSG measurement section below). After the electrodes were
449 attached, each sleep session started in the early afternoon for simultaneous measurement of MRI
450 and PSG (see the MRI acquisition section below). The sleep session was conducted for
451 approximately 90 min in the MRI scanner. After the sleep session, they answered a questionnaire
452 about the sleep content (data not shown).

453 The participants were instructed to maintain their regular sleep-wake habits, i.e., their daily
454 wake/sleep time and sleep duration, until the study was over. The sleep-wake habits of the
455 participants were monitored by a sleep log and an actigraphy device (ACOS, Japan) during the
456 study. Throughout their participation, the subjects were instructed to refrain from taking naps. One
457 day prior to the experiments, alcohol consumption was not allowed. Unusual excessive physical
458 exercise and caffeine consumption were not allowed on the day of the sleep sessions.

459

460 ***MRI acquisition***

461 MRI data were acquired with a 3T Siemens Prisma MRI scanner (Siemens Healthineers, Germany)
462 using a 64-channel head and neck coil at RIKEN. An anatomical T1-weighted image was acquired

using a 3D magnetization-prepared rapid gradient echo (MPRAGE) sequence (TR = 2180 ms, TI = 1100 ms, TE = 2.95 ms, FA = 8°, voxel size = 0.7×0.7×0.7 mm^3, FOV = 290 × 320 × 256 mm). Functional MRI data were acquired using a sparse gradient-echo echo-planar imaging sequence (TR/TE=3000/30 ms, FA=85°, Multiband factor=3, 42 transverse slices, voxel size = 3x3x3 mm^3, 1800 volumes, GRAPPA factor=3, bandwidth=752 Hz/pixel, B1+RMS=0.5 μT, MR acquisition time=0.9 s, and quiet period=2.1 s)[59]. Cardiac and respiratory cycles were simultaneously recorded using a fingertip PPG sensor and respiratory belt (BIOPAC, US) with a 100 Hz sampling rate. Anatomical and functional MRI data were acquired simultaneously with polysomnography (see the PSG measurement section below). Cushions and gauze were used to stabilize the subjects' heads to reduce discomfort and head motion. Back and knee cushions were used upon the participants' request to further reduce discomfort. Several blankets were used to keep the participants warm and to initiate sleep during the scan[23,32].

PSG measurement

EEG data were acquired using a BrainAmp MRplus EEG amplifier (Brain Products, Gilching, Germany) with a 5 kHz sampling rate and an MR-compatible 32-channel EEG cap (EasyCap, Wörthsee, Germany). The hardware bandpass filters were set to a 0.016–250 Hz range, with a roll-off of 30 dB/octave at high frequency. The electrode layout followed the extended international 10-20 system with additional drop-down channels or bipolar electrodes for recording the electrocardiogram (ECG), electrooculogram (EOG), and chin electromyogram (EMG). EEG was measured from either 27 electrodes (16 participants) or 31 electrodes (9 participants). For all of the participants, EOG was measured from electrodes placed at the outer canthi. EMG was measured from the mentum. ECG signals were measured from the lower shoulder blade. FCz was

used as the reference electrode, whereas AFz was used as the ground electrode. EEG data were transferred outside the scanner room through fiber optic cables to a computer running the BrainVision Recorder software (Brain Products, Gilching, Germany). MR-EEG scanner clocks were synchronized (Brain Products Synchbox) for all EEG data acquisitions, and the onset of every scanner repetition time (TR) period was recorded in the EEG data for MR gradient artifact correction. The impedance of all electrodes was initially maintained below 10 kΩ and was maintained below a maximum of 20 kΩ for the duration of the study.

PSG data preprocessing

PSG data were contaminated by artifacts due to the strong magnetic field. To remove the artifacts from the PSG data, gradient artifacts were first corrected using BrainVision Analyzer2 (Version 2.2.0, Brain Products GmbH, Gilching, Germany) with the standard average artifact subtraction (AAS) method. The AAS method uses sliding window templates formed from the averages of 21 TRs, which are subtracted from each occurrence of the respective artifacts for each electrode [60,61]. The gradient-artifact corrected data were subsequently bandpass filtered (EEG: 0.1–50 Hz with a notch filter of 50 Hz) and downsampled to 250 Hz. Following the GA correction, cardiac R-peaks were automatically detected from the ECG recording in BrainVision Analyzer2, checked visually and corrected manually if necessary. These R-peak events were used to inform ballistocardiogram correction. The BCG artifacts were further corrected via the AAS method with sliding window templates formed from the averages of 21 R-peaks in BrainVision Analyzer2[62,63]. These procedures were conducted for the whole duration of the fMRI scan to obtain artifact-removed PSG data for further processing (see ***Sleep stage scoring*** and ***Sleep event detection*** below).

Sleep stage scoring

Sleep staging was conducted on the artifact-removed PSG data following the standard criteria[35]. Prior to sleep staging, PSG data were further bandpass filtered between 0.3 and 40 Hz for EEG, EOG and ECG and between 10 and 50 Hz for EMG to remove low-frequency drift and high-frequency noise and were re-referenced to the linked mastoids (TP9 & TP10). Scoring of the sleep stages was performed every 30 s in conjunction by two trained sleep scorers (MT & AS). We obtained sleep parameters, including the total sleep time and duration of the sleep stages (**Table 1**). For further analysis, N1 and N2 were combined as light NREM sleep, and N3 was categorized as slow-wave sleep. Epochs with motion artifacts and arousal events were marked and removed from further analyses, whereas the arousal events were used only for arousal analysis.

Sleep event detection

Using the artifact-removed PSG data, sleep events, including slow waves, sleep spindles, rapid eye movements, sawtooth waves, and arousal events, were detected as follows.

<u>Slow waves</u>

Slow waves were detected using a two-step semiautomatic procedure. First, slow waves were detected automatically[64] using Wonambi software (https://wonambi-python.github.io/) for the F3, Fz, F4, C3, Cz, C4, P3, Pz, and P4 electrodes during the N2 and N3 stages. Specifically, EEG signals were bandpass filtered between 0.1 and 4 Hz with a zero-phase 4th-order Butterworth filter. Slow waves were detected when the following three criteria were met: 1) a positive-to-negative zero crossing and a subsequent negative-to-positive zero crossing separated between 0.3 s and 1 s, 2) a negative peak between the two zero crossings with voltages smaller than -80 μV, and 3) a

peak-to-peak amplitude greater than 140 μV. The automatically detected slow waves were then reviewed and removed by an experimenter if necessary. The number of slow waves was measured for each electrode, and the electrode that had the maximum number of slow waves was used as the most sensitive electrode for slow wave detection. The onset and duration of slow waves were measured from the specific electrode for further analysis of CSF and GM signals (see ***fMRI time course analysis*** and ***fMRI GLM analysis*** below).

Sleep spindles

Spindles were detected using a two-step semiautomatic procedure. As the first step, an automatic spindle detection method was used to detect the spindles[65] with Wonambi software for the F3, Fz, F4, C3, Cz, C4, P3, Pz, and P4 electrodes during the N2 and N3 stages. Specifically, these EEG signals were filtered between 12–15 Hz, which corresponded to the sleep spindle frequency band. The root mean square (RMS) of the filtered signals was subsequently calculated at every sample point using a moving window of 0.2 s. The threshold for spindle detection in the RMS signal was set to 1.5 standard deviations of the filtered signal for each electrode. A spindle was detected when the RMS signal remained above the threshold for 0.5–3 s, and then the beginning and end of the spindle were marked at the threshold crossing points. When sleep spindles from multiple electrodes overlapped within a 5 s time window, those sleep spindles were treated as trains of continuous sleep spindles and merged. In the second step, the automatically detected spindles were reviewed and removed by an experimenter if necessary. The onset and duration of sleep spindles were used for further analysis of CSF and GM signals (see ***fMRI time course analysis*** and ***fMRI GLM analysis*** below).

555 Rapid eye movements

556 Rapid eye movement events were detected during REM sleep. Rapid eye movement events were
557 automatically detected on two EOG signals[66]. Specifically, to separate rapid eye movements from
558 slow eye movements (SEMs), two channels of EOG data are filtered using a fourth-order
559 Butterworth bandpass filter with cutoffs at 1 and 9 Hz to yield the filtered EOG data. The candidate
560 REM sleep events were generated as the negative instantaneous product of the two filtered EOG
561 sequences, and the REM sleep events were detected on the basis of their amplitude threshold. The
562 amplitude threshold was arbitrarily determined on the basis of each individual dataset, since, owing
563 to differences in the setup and/or the quality of the artifact removal, there were individual
564 differences in the amplitude of the EOG data. The onset and duration of rapid eye movements were
565 used for further analysis of the CSF and GM signals (see ***fMRI time course analysis*** below).

566

567 Sawtooth waves

568 Sawtooth waves were manually marked on the scalp EEG independently by two trained sleep
569 scores (MT & SA) for the REM sleep episodes. These waves were defined as bursts of consecutive
570 surface-positive 2–5 Hz frontocentral bilateral synchronous symmetric waves with amplitudes of
571 20–100 μV and with a slow incline to a negative peak with a subsequent steep linear decline ending
572 at a positive peak[67–69]. The minimum number of consecutive waves was set as 3. The consensus of
573 the markings obtained from the two raters was selected, and the onset and duration of sawtooth
574 waves were used for further analysis of the CSF and GM signals (see ***fMRI timecourse analysis***
575 below).

576

577 Arousals

An arousal was defined as an abrupt shift in EEG frequency, which may include theta, alpha and/or frequencies greater than 16 Hz (but not spindles) that were at least 3 seconds in duration, with at least 10 seconds of stable sleep preceding the change, in accordance with the standard AASM criteria[35]. Arousal events were manually scored by two trained sleep experts (MT & SA) by visually checking the EEG signals. The consensus of the arousal scoring was used, and the onset and duration of arousal were used for further analysis of the CSF and GM signals (see ***fMRI time course analysis*** and ***fMRI GLM analysis*** below).

MRI data analysis

High-resolution T1-weighted images were processed using FreeSurfer 7.4.0[70] (https://surfer.nmr.mgh.harvard.edu/fswiki/FreeSurferWiki) to segment the head into five tissues (i.e., the scalp, skull, cerebrospinal fluid (CSF), gray matter and white matter), and an anatomical atlas. Anatomical surfaces such as the pial surface, gray/white matter interface and mid surface (i.e., a middle layer of the gray matter) were estimated using FreeSurfer[71]. The whole gray matter region (GM) and lateral ventricles were extracted as the two main regions of interest (ROIs) from each individual participant's anatomical image. For control analyses, the MRI signals were also extracted from the fourth ventricles (see the **Supplementary Note**). The fMRI data were motion-corrected and slice-timing corrected using the AFNI (https://afni.nimh.nih.gov) and RIKEN fMRI processing programs (http://www.fmri.brain.riken.jp/~mri/Software.html). Furthermore, the fMRI data were denoised using cardiac and respiration signals[33,34]. The two ROI images (GM and lateral ventricles) were subsequently registered to each fMRI image using FSL FLIRT (https://fsl.fmrib.ox.ac.uk/fsl/fslwiki/FLIRT), and the fMRI signals were z score transformed and averaged across the voxels inside each ROI for each sleep session and each participant.

601

602 ***Power spectrum analysis of fMRI data***

603 Time-frequency analysis was applied to the whole fMRI signals during a sleep session of the two
604 ROIs using a multitaper approach[59,72] in the Fieldtrip toolbox[73]
605 (http://www.ru.nl/neuroimaging/fieldtrip). Time windows of 200 s duration were moved across the
606 data in steps of 3 s corresponding to 1 TR, resulting in a frequency resolution of 0.005 Hz. The
607 calculated time-frequency representations (TFRs) were then transformed to the scale of dB by
608 10*log10, then demeaned by subtracting the mean power at each frequency during the whole
609 recording to calculate power fluctuations. Then, they were segmented based on sleep stages every
610 30 s, and averaged across each 30 s to extract each epoch power spectrum after removing arousal-
611 and motion-contaminated epochs. On the basis of the resulting power spectrum, periodic
612 components of the power spectrum were extracted after the estimated 1/f aperiodic components
613 were removed by fitting oscillations and one-over-f (FOOOF) algorithms[74]. The resulting periodic
614 power spectra were averaged for each sleep stage first and then across sleep sessions for each ROI.

615

616 ***Power spectrum analysis of cardiac and respiration signals***

617 Cardiac and respiratory cycles during each sleep session were recorded using a fingertip PPG
618 sensor and respiratory belt (BIOPAC, US) with a 100 Hz sampling rate. The same power spectrum
619 analysis steps were applied to the cardiac and respiration signals (see ***Power spectrum analysis of***
620 ***fMRI data*** above).

621

622 ***fMRI time course analysis***

fMRI data in each ROI were segmented based on sleep events (slow waves, spindles, rapid eye movements, sawtooth waves, and arousals). First, -9–0 s (3TRs) before the onset of the events was defined as a baseline. This baseline signal was averaged and subtracted from 0–30 s after the onset of the events. These data were averaged across the number of each event for each sleep session and then averaged across the sleep sessions and participants.

Cardiac and respiration peak-related fMRI time course analysis

Cardiac and respiratory cycles during each sleep session were recorded using a fingertip PPG sensor and respiratory belt (BIOPAC, US) with a 100 Hz sampling rate. Peaks of the cardiac and respiration cycles were detected using RIKEN fMRI processing programs (http://www.fmri.brain.riken.jp/~mri/Software.html). fMRI data in each ROI were segmented based on the peaks of the cardiac and respiration signals. First, -9–0 s (3TRs) before the onset of the peak events was defined as a baseline. This baseline signal was averaged and subtracted from 0–30 s after the onset of the peak events. These data were averaged across the number of each event for each sleep session and then averaged across the sleep sessions and participants.

fMRI GLM analysis

MRI data were processed using FSL v6.0.7.7 (https://fsl.fmrib.ox.ac.uk/fsl/). Data from each participant were motion corrected (MCFLIRT), spatially smoothed (5 mm FWHM Gaussian kernel), high-pass temporally filtered (100 s cutoff), registered to their T1 anatomical brain image (FLIRT), and normalized to the MNI 2 mm standard brain. GLM analyses were performed using FEAT v6.00. On the basis of each sleep-specific event (onset and duration for slow waves, sleep spindles, and arousals) detected from the simultaneous EEG data, event-specific first-level analysis

was performed employing one regressor: 1) the event onset and duration. The regressor of interest was convolved with the double-gamma HRF. Motion parameters estimated during image realignment (3 translations and 3 rotations around the x, y, and z axes) were included in the matrix as confounding regressors of no interest. Additionally, since MRI BOLD signal amplitudes vary across different vigilance states, including sleep[9,10,75–78], the mean MRI signal inside the white matter region and the mean MRI signal in the cerebrospinal fluid region were included in the GLM as nuisance regressors[79]. For each event of each participant, the event-specific first-level results were combined across sleep sessions using a second-level, fixed effect analysis to calculate an average response per subject. For each event, these second-level results were subsequently combined and analyzed at the group level using a FLAME mixed-effect analysis[80]. In a cluster-based threshold statistical analysis, the resulting group-level BOLD Z statistic images were thresholded using $Z > 3.1$ and a cluster-corrected significance threshold of $P < 0.05$. For visualization, the group-level thresholded significant BOLD Z statistic image for each event (slow waves, sleep spindles, and arousals) was transformed onto a standard template surface map (fsaverage) using feat2surf and a standard template subcortical brain region, and the group-level thresholded significant BOLD Z statistic image was shown as an isosurface in 3D view in FreeSurfer freeview software. The automated anatomical atlas 3 (AAL3[81]) was used for anatomical labeling.

Correlation analysis between CSF and GM signals

Sleep-specific event-locked (i.e., slow waves, spindles, and REM sleep events) time courses of the CSF and GM signals based on their onset times (-9 s to 30 s) were used to investigate the

correlations between the CSF and GM signals. The correlation coefficients and time lags were extracted when the absolute coefficient values were at their maximum between the two signals.

CSF peak locked EEG topography analysis

Positive peaks of the CSF signal from the lateral ventricles during each sleep session were detected using a MATLAB function (findpeaks.m). The MRI-related artifact-removed EEG data were segmented based on the positive peak events of the CSF signals (-10 s to 0 s). The segmented EEG data were averaged across the sleep sessions and participants for each sleep stage (N2 and N3 sleep stages). EEG topographies across time were generated in the Fieldtrip toolbox [73] (http://www.ru.nl/neuroimaging/fieldtrip).

Statistical analysis

For the fMRI power spectrum analysis, nonparametric cluster-based permutation tests were used to find significant differences ($P < 0.05$) in the periodic power spectrum across different sleep stages in each ROI using the Fieldtrip toolbox[82–84]. For the fMRI time course analysis, two-tailed one-sample *t*-tests ($P < 0.05$) were applied to each time point of the fMRI signals compared with zero. Two-tailed paired *t*-tests were used to compare each time point of event-locked fMRI signals between sleep stages. Two-tailed paired *t*-tests were used for the statistical inference of the correlation analysis and the numbers and time intervals of each event across different sleep depths. The alpha level was set as 0.05. To control for multiple comparison problems, Bonferroni corrections were applied to minimize the false-positive rates in the statistical inference of the correlation analysis and the numbers and time intervals of each event across different sleep depths.

690 False discovery rate (FDR) corrections[85] were used for other statistical comparisons, such as
691 comparing each time point of the fMRI signals.
692

693 ***Data availability***

694 The datasets generated and/or analyzed in the current study are available from the
695 corresponding author upon request.

696

697 ***Code availability***

698 The computer code that was used to generate results central to the conclusions of this
699 study is available from the corresponding author upon request.

700

701 **Acknowledgements**

702 The authors thank M. A. Carskadon for helpful comments on an earlier draft. This work
703 was supported by JSPS KAKENHI Grant Numbers JP22H01107 (MT) and JP22K18664 (MT),
704 the Naito Foundation (MT), Takeda Science Foundation (MT), Life Science Foundation of
705 JAPAN (MU).

706

707 **Author contributions**

708 MU and MT designed the research. MU, XL, AS, RK, RAW, CS, KU, SA and MT
709 performed the experiments. MU, SA and MT analyzed the data. MU and MT wrote the paper.
710 All confirmed the content.

711

712 **Competing interests**

The authors declare no competing interests.

Supplementary Materials:

Supplementary Figs. S1–16

Supplementary Tables S1–7

Supplementary Note

References

1. Stickgold, R. Sleep-dependent memory consolidation. *Nature* **437**, 1272–1278 (2005).
2. Marshall, L., Helgadóttir, H., Mölle, M. & Born, J. Boosting slow oscillations during sleep potentiates memory. *Nature* **444**, 610–613 (2006).
3. Krause, A. J. *et al.* The sleep-deprived human brain. *Nat Rev Neurosci* **18**, 404–418 (2017).
4. Irwin, M. R. & Vitiello, M. V. Implications of sleep disturbance and inflammation for Alzheimer's disease dementia. *Lancet Neurol* **18**, 296–306 (2019).
5. Xie, L. *et al.* Sleep Drives Metabolite Clearance from the Adult Brain. *Science (1979)* **342**, 373–377 (2013).
6. Eide, P. K., Vinje, V., Pripp, A. H., Mardal, K.-A. & Ringstad, G. Sleep deprivation impairs molecular clearance from the human brain. *Brain* **144**, 863–874 (2021).
7. Iliff, J. J. *et al.* A Paravascular Pathway Facilitates CSF Flow Through the Brain Parenchyma and the Clearance of Interstitial Solutes, Including Amyloid β. *Sci Transl Med* **4**, (2012).
8. Eide, P. K. *et al.* Altered glymphatic enhancement of cerebrospinal fluid tracer in individuals with chronic poor sleep quality. *Journal of Cerebral Blood Flow & Metabolism* **42**, 1676–1692 (2022).
9. Fultz, N. E. *et al.* Coupled electrophysiological, hemodynamic, and cerebrospinal fluid oscillations in human sleep. *Science (1979)* **366**, 628–631 (2019).
10. Picchioni, D. *et al.* Autonomic arousals contribute to brain fluid pulsations during sleep. *Neuroimage* **249**, 118888 (2022).
11. Gonzalez-Castillo, J., Fernandez, I. S., Handwerker, D. A. & Bandettini, P. A. Ultra-slow fMRI fluctuations in the fourth ventricle as a marker of drowsiness. *Neuroimage* **259**, 119424 (2022).
12. de Zambotti, M. *et al.* K-Complexes: Interaction between the Central and Autonomic Nervous Systems during Sleep. *Sleep* **39**, 1129–1137 (2016).
13. Tank, J. *et al.* Relationship between blood pressure, sleep K-complexes, and muscle sympathetic nerve activity in humans. *American Journal of Physiology-Regulatory, Integrative and Comparative Physiology* **285**, R208–R214 (2003).
14. Latreille, V. *et al.* The human K-complex: Insights from combined scalp-intracranial EEG recordings. *Neuroimage* **213**, 116748 (2020).
15. Wang, Y. L. *et al.* Intracerebral dynamics of sleep arousals: a combined scalp-intracranial EEG study. *The Journal of Neuroscience* e0617232024 (2024) doi:10.1523/JNEUROSCI.0617-23.2024.
16. Mander, B. A., Winer, J. R. & Walker, M. P. Sleep and Human Aging. *Neuron* **94**, 19–36 (2017).
17. Mander, B. A. *et al.* Prefrontal atrophy, disrupted NREM slow waves and impaired hippocampal-dependent memory in aging. *Nat Neurosci* **16**, 357–364 (2013).
18. Lendner, J. D. *et al.* Human REM sleep recalibrates neural activity in support of memory formation. *Sci Adv* **9**, (2023).
19. Stickgold, R., James, L. & Hobson, J. A. Visual discrimination learning requires sleep after training. *Nat Neurosci* **3**, 1237–1238 (2000).

20. Peigneux, P. *et al.* Learned material content and acquisition level modulate cerebral reactivation during posttraining rapid-eye-movements sleep. *Neuroimage* **20**, 125–134 (2003).
21. Durrant, S. J., Cairney, S. A., McDermott, C. & Lewis, P. A. Schema-conformant memories are preferentially consolidated during REM sleep. *Neurobiol Learn Mem* **122**, 41–50 (2015).
22. Cairney, S. A., Durrant, S. J., Power, R. & Lewis, P. A. Complementary Roles of Slow-Wave Sleep and Rapid Eye Movement Sleep in Emotional Memory Consolidation. *Cerebral Cortex* **25**, 1565–1575 (2015).
23. Tamaki, M. *et al.* Complementary contributions of non-REM and REM sleep to visual learning. *Nat Neurosci* **23**, 1150–1156 (2020).
24. McCormick, D. A. & Bal, T. SLEEP AND AROUSAL: Thalamocortical Mechanisms. *Annu Rev Neurosci* **20**, 185–215 (1997).
25. Andrillon, T. *et al.* Sleep Spindles in Humans: Insights from Intracranial EEG and Unit Recordings. *The Journal of Neuroscience* **31**, 17821–17834 (2011).
26. Nir, Y. *et al.* Regional Slow Waves and Spindles in Human Sleep. *Neuron* **70**, 153–169 (2011).
27. Boyce, R., Glasgow, S. D., Williams, S. & Adamantidis, A. Causal evidence for the role of REM sleep theta rhythm in contextual memory consolidation. *Science (1979)* **352**, 812–816 (2016).
28. Jiang-Xie, L.-F. *et al.* Neuronal dynamics direct cerebrospinal fluid perfusion and brain clearance. *Nature* **627**, 157–164 (2024).
29. Rechtschaffen, A. & Kales, A. *A Manual of Standardized Terminology, Techniques and Scoring System of Sleep Stages in Human Subjects*. (Public Health Service, US Government Printing Office, Washington DC, 1968).
30. Özbay, P. S. *et al.* Sympathetic activity contributes to the fMRI signal. *Commun Biol* **2**, 421 (2019).
31. Moehlman, T. M. *et al.* All-night functional magnetic resonance imaging sleep studies. *J Neurosci Methods* **316**, 83–98 (2019).
32. Tamaki, M., Watanabe, T. & Sasaki, Y. Coregistration of magnetic resonance spectroscopy and polysomnography for sleep analysis in human subjects. *STAR Protoc* **2**, 100974 (2021).
33. Hu, X., Le, T. H., Parrish, T. & Erhard, P. Retrospective estimation and correction of physiological fluctuation in functional MRI. *Magn Reson Med* **34**, 201–212 (1995).
34. Glover, G. H., Li, T.-Q. & Ress, D. Image-based method for retrospective correction of physiological motion effects in fMRI: RETROICOR. *Magn Reson Med* **44**, 162–167 (2000).
35. Berry, R., Quan, S. & Abreu, A. Manual for the Scoring of Sleep and Associated Events: Rules, Terminology and Technical Specifications. *American Academy of Sleep Medicine* **Version 2.6**, (2020).
36. Williams, S. D. *et al.* Neural activity induced by sensory stimulation can drive large-scale cerebrospinal fluid flow during wakefulness in humans. *PLoS Biol* **21**, e3002035 (2023).
37. Adamantidis, A. R., Gutierrez Herrera, C. & Gent, T. C. Oscillating circuitries in the sleeping brain. *Nat Rev Neurosci* **20**, 746–762 (2019).
38. Horikawa, T., Tamaki, M., Miyawaki, Y. & Kamitani, Y. Neural Decoding of Visual Imagery During Sleep. *Science (1979)* **340**, 639–642 (2013).

39. Miyauchi, S., Misaki, M., Kan, S., Fukunaga, T. & Koike, T. Human brain activity time-locked to rapid eye movements during REM sleep. *Exp Brain Res* **192**, 657–667 (2009).
40. Strik, C., Klose, U., Erb, M., Strik, H. & Grodd, W. Intracranial oscillations of cerebrospinal fluid and blood flows: Analysis with magnetic resonance imaging. *Journal of Magnetic Resonance Imaging* **15**, 251–258 (2002).
41. Borbely, A. A. A two process model of sleep regulation. *Hum Neurobiol* **1**, (1982).
42. Brodt, S., Inostroza, M., Niethard, N. & Born, J. Sleep—A brain-state serving systems memory consolidation. *Neuron* **111**, 1050–1075 (2023).
43. Tononi, G. & Cirelli, C. Sleep and the Price of Plasticity: From Synaptic and Cellular Homeostasis to Memory Consolidation and Integration. *Neuron* **81**, 12–34 (2014).
44. Halász, P., Terzano, M., Parrino, L. & Bódizs, R. The nature of arousal in sleep. *J Sleep Res* **13**, 1–23 (2004).
45. Fogel, S. *et al.* Reactivation or transformation? Motor memory consolidation associated with cerebral activation time-locked to sleep spindles. *PLoS One* **12**, e0174755 (2017).
46. Tamaki, M., Matsuoka, T., Nittono, H. & Hori, T. Fast Sleep Spindle (13–15 Hz) Activity Correlates with Sleep-Dependent Improvement in Visuomotor Performance. *Sleep* **31**, 204–211 (2008).
47. Schabus, M. *et al.* Interindividual sleep spindle differences and their relation to learning-related enhancements. *Brain Res* **1191**, 127–135 (2008).
48. Ungurean, G. *et al.* Wide-spread brain activation and reduced CSF flow during avian REM sleep. *Nat Commun* **14**, 3259 (2023).
49. Bojarskaite, L. *et al.* Sleep cycle-dependent vascular dynamics in male mice and the predicted effects on perivascular cerebrospinal fluid flow and solute transport. *Nat Commun* **14**, 953 (2023).
50. Turner, K. L., Gheres, K. W., Proctor, E. A. & Drew, P. J. Neurovascular coupling and bilateral connectivity during NREM and REM sleep. *Elife* **9**, (2020).
51. Chen, L., Beckett, A., Verma, A. & Feinberg, D. A. Dynamics of respiratory and cardiac CSF motion revealed with real-time simultaneous multi-slice EPI velocity phase contrast imaging. *Neuroimage* **122**, 281–287 (2015).
52. Vijayakrishnan Nair, V. *et al.* Human CSF movement influenced by vascular low frequency oscillations and respiration. *Front Physiol* **13**, (2022).
53. Slutsky, I. Linking activity dyshomeostasis and sleep disturbances in Alzheimer disease. *Nat Rev Neurosci* **25**, 272–284 (2024).
54. Ju, Y.-E. S. *et al.* Sleep Quality and Preclinical Alzheimer Disease. *JAMA Neurol* **70**, 587 (2013).
55. Vitiello, M. V., Prinz, P. N., Williams, D. E., Frommlet, M. S. & Ries, R. K. Sleep Disturbances in Patients With Mild-Stage Alzheimer's Disease. *J Gerontol* **45**, M131–M138 (1990).
56. Liu, G., Ladrón-de-Guevara, A., Izhiman, Y., Nedergaard, M. & Du, T. Measurements of cerebrospinal fluid production: a review of the limitations and advantages of current methodologies. *Fluids Barriers CNS* **19**, 101 (2022).
57. Buysse, D. J., Reynolds, C. F., Monk, T. H., Berman, S. R. & Kupfer, D. J. The Pittsburgh sleep quality index: A new instrument for psychiatric practice and research. *Psychiatry Res* **28**, 193–213 (1989).
58. Hoddes, E., Zarcone, V., Smythe, H., Phillips, R. & Dement, W. C. Quantification of Sleepiness: A New Approach. *Psychophysiology* **10**, 431–436 (1973).

59. Uji, M., Wilson, R., Francis, S. T., Mullinger, K. J. & Mayhew, S. D. Exploring the advantages of multiband fMRI with simultaneous EEG to investigate coupling between gamma frequency neural activity and the BOLD response in humans. *Hum Brain Mapp* **39**, 1673–1687 (2018).
60. Allen, P. J., Josephs, O. & Turner, R. A Method for Removing Imaging Artifact from Continuous EEG Recorded during Functional MRI. *Neuroimage* **12**, 230–239 (2000).
61. Wilson, R., Mullinger, K. J., Francis, S. T. & Mayhew, S. D. The relationship between negative BOLD responses and ERS and ERD of alpha/beta oscillations in visual and motor cortex. *Neuroimage* **199**, 635–650 (2019).
62. Bullock, M., Jackson, G. D. & Abbott, D. F. Artifact Reduction in Simultaneous EEG-fMRI: A Systematic Review of Methods and Contemporary Usage. *Front Neurol* **12**, (2021).
63. Warbrick, T. Simultaneous EEG-fMRI: What Have We Learned and What Does the Future Hold? *Sensors* **22**, 2262 (2022).
64. Massimini, M., Huber, R., Ferrarelli, F., Hill, S. & Tononi, G. The Sleep Slow Oscillation as a Traveling Wave. *The Journal of Neuroscience* **24**, 6862–6870 (2004).
65. Mölle, M., Bergmann, T. O., Marshall, L. & Born, J. Fast and Slow Spindles during the Sleep Slow Oscillation: Disparate Coalescence and Engagement in Memory Processing. *Sleep* **34**, 1411–1421 (2011).
66. Agarwal, R., Takeuchi, T., Laroche, S. & Gotman, J. Detection of Rapid-Eye Movements in Sleep Studies. *IEEE Trans Biomed Eng* **52**, 1390–1396 (2005).
67. Frauscher, B. *et al.* Rapid Eye Movement Sleep Sawtooth Waves Are Associated with Widespread Cortical Activations. *The Journal of Neuroscience* **40**, 8900–8912 (2020).
68. Peter-Derex, L. *et al.* Enhanced thalamocortical functional connectivity during rapid-eye-movement sleep sawtooth waves. *Sleep* **46**, (2023).
69. Sato, S. *et al.* Relationship between muscle tone changes, sawtooth waves and rapid eye movements during sleep. *Electroencephalogr Clin Neurophysiol* **103**, 627–632 (1997).
70. Fischl, B. FreeSurfer. *Neuroimage* **62**, 774–781 (2012).
71. Fischl, B. & Dale, A. M. Measuring the thickness of the human cerebral cortex from magnetic resonance images. *Proceedings of the National Academy of Sciences* **97**, 11050–11055 (2000).
72. Scheeringa, R. *et al.* Neuronal Dynamics Underlying High- and Low-Frequency EEG Oscillations Contribute Independently to the Human BOLD Signal. *Neuron* **69**, 572–583 (2011).
73. Oostenveld, R., Fries, P., Maris, E. & Schoffelen, J.-M. FieldTrip: Open Source Software for Advanced Analysis of MEG, EEG, and Invasive Electrophysiological Data. *Comput Intell Neurosci* **2011**, 1–9 (2011).
74. Donoghue, T. *et al.* Parameterizing neural power spectra into periodic and aperiodic components. *Nat Neurosci* **23**, 1655–1665 (2020).
75. Fukunaga, M. *et al.* Large-amplitude, spatially correlated fluctuations in BOLD fMRI signals during extended rest and early sleep stages. *Magn Reson Imaging* **24**, 979–992 (2006).
76. Horovitz, S. G. *et al.* Low frequency BOLD fluctuations during resting wakefulness and light sleep: A simultaneous EEG-fMRI study. *Hum Brain Mapp* **29**, 671–682 (2008).
77. Larson-Prior, L. J. *et al.* Cortical network functional connectivity in the descent to sleep. *Proceedings of the National Academy of Sciences* **106**, 4489–4494 (2009).

78. Olbrich, S. *et al.* EEG-vigilance and BOLD effect during simultaneous EEG/fMRI measurement. *Neuroimage* **45**, 319–332 (2009).
79. Caballero-Gaudes, C. & Reynolds, R. C. Methods for cleaning the BOLD fMRI signal. *Neuroimage* **154**, 128–149 (2017).
80. Woolrich, M. W., Behrens, T. E. J., Beckmann, C. F., Jenkinson, M. & Smith, S. M. Multilevel linear modelling for FMRI group analysis using Bayesian inference. *Neuroimage* **21**, 1732–1747 (2004).
81. Rolls, E. T., Huang, C.-C., Lin, C.-P., Feng, J. & Joliot, M. Automated anatomical labelling atlas 3. *Neuroimage* **206**, 116189 (2020).
82. Maris, E. Statistical testing in electrophysiological studies. *Psychophysiology* **49**, 549–565 (2012).
83. Maris, E. & Oostenveld, R. Nonparametric statistical testing of EEG- and MEG-data. *J Neurosci Methods* **164**, 177–190 (2007).
84. Nichols, T. E. & Holmes, A. P. Nonparametric permutation tests for functional neuroimaging: A primer with examples. *Hum Brain Mapp* **15**, 1–25 (2002).
85. Genovese, C. R., Lazar, N. A. & Nichols, T. Thresholding of Statistical Maps in Functional Neuroimaging Using the False Discovery Rate. *Neuroimage* **15**, 870–878 (2002).

922

Table 1 Sleep parameters

	NP	NS	Mean ± SE		
Time in bed (min)	25	50	89.7	±	0.3
Sleep efficiency (%)	25	50	77.6	±	3.2
Wakefulness (%)	25	48	22.4	±	3.2
Light NREM sleep (%)	25	50	62.8	±	2.9
Slow-wave sleep (%)	18	30	12.3	±	2.3
REM sleep (%)	13	18	2.4	±	0.6

NP, the number of participants. **NS**, the number of sessions. Time in bed indicates the duration of sleep sessions during MRI scan (the time interval between lights-off and lights-on). Sleep efficiency was measured by [total sleep duration / time in bed]. Light NREM sleep indicates the percentage of time in NREM sleep stages 1 and 2. Slow-wave sleep indicates the percentage of time in NREM sleep stage 3. REM sleep indicates the percentage of time in REM sleep stage. PSG data were scored in accordance with standard criteria[35].

923
924

925

Table 2: Summary of key oscillations, recruited brain regions, and CSF characteristics during sleep and arousals.

	Light NREM sleep	**Slow-wave sleep**	**REM sleep**	**Arousals**
Key oscillations / events	K-complexes Sleep spindles	Slow waves Sleep spindles	Rapid eye movements Sawtooth waves	N/A (mixed)
Brain regions	Sensory	Frontal, hippocampus	Visual, hippocampus	Widespread
CSF frequency	Slow	Fast	Slow + very fast	N/A
CSF amplitude	Larger	Smaller	Larger	Larger
CSF latency	Longer	Shorter	Longer	Longer

Brain regions indicate activated brain regions to key oscillations or events in each sleep stage. CSF power frequency indicates the frequency characteristics in each sleep stage. CSF amplitude and latency indicates relative amplitudes and latencies in the CSF signals time-locked to the onset of brain oscillations / events across different sleep stages. **Green** cells indicate slower and larger impacts on the CSF signals, representing strong but infrequent CSF and brain dynamics. **Blue** cells indicate faster and smaller impacts on the CSF signals, representing mild but frequent CSF and brain dynamics. **Red** cell indicates a very fast component in the CSF signals that is specific to REM sleep with a mixture of the slow component (green).

926
927

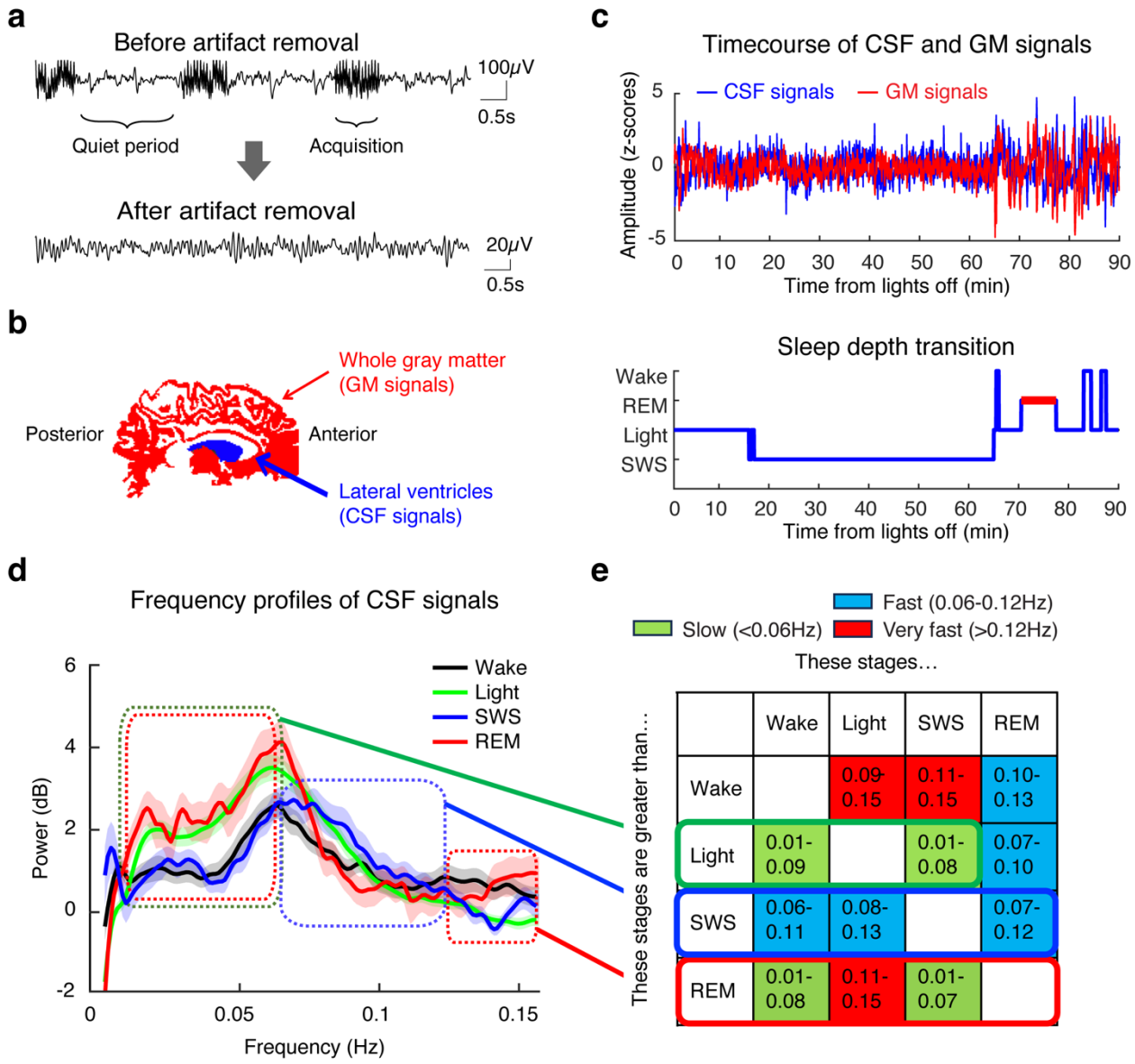

Fig. 1: Frequency profiles of CSF signals in the lateral ventricles vary across different sleep depths. a, Example EEG data before and after artifact removal obtained via the sparse fMRI method developed in the present study. **b**, A schematic of the regions of interest. Blue, lateral ventricles. Red, whole gray matter (GM). **c**, Example MRI signals (top) and corresponding sleep stages (bottom) during a 90-min sleep session. Blue, CSF signals. Red, GM signals. Wake, wakefulness. SWS, slow-wave sleep. Light, light NREM sleep. REM, REM sleep. **d**, Periodic CSF

signal power spectrum against each frequency bin for each sleep stage. The fast component power was significantly greater during slow-wave sleep than during wakefulness or light NREM sleep (blue vs. green and black; cluster-based permutation tests, *Ps* < 0.05; **Supplementary Fig. S1b & d**). In contrast, the slow component was significantly larger during light NREM than during wakefulness or slow-wave sleep (green vs. black and blue; cluster-based permutation tests, *P* < 0.05; **supplementary Fig. S1a & d**). See **Supplementary Fig. S1** for detailed comparisons across sleep stages and frequencies. Wake, wakefulness. SWS, slow-wave sleep. Light, light NREM sleep. REM, REM sleep. **e**, Summary of significant differences in the CSF frequency profiles across different sleep stages. The values indicate the ranges of frequencies where significant differences were found by cluster-based permutation tests (*Ps* < 0.05) among sleep stages. The fast component dominates slow-wave sleep (blue), whereas REM sleep shows a mixture of slow and very fast components (red). The slow components dominate light NREM sleep (green). Wake, wakefulness. SWS, slow-wave sleep. Light, light NREM sleep. REM, REM sleep.

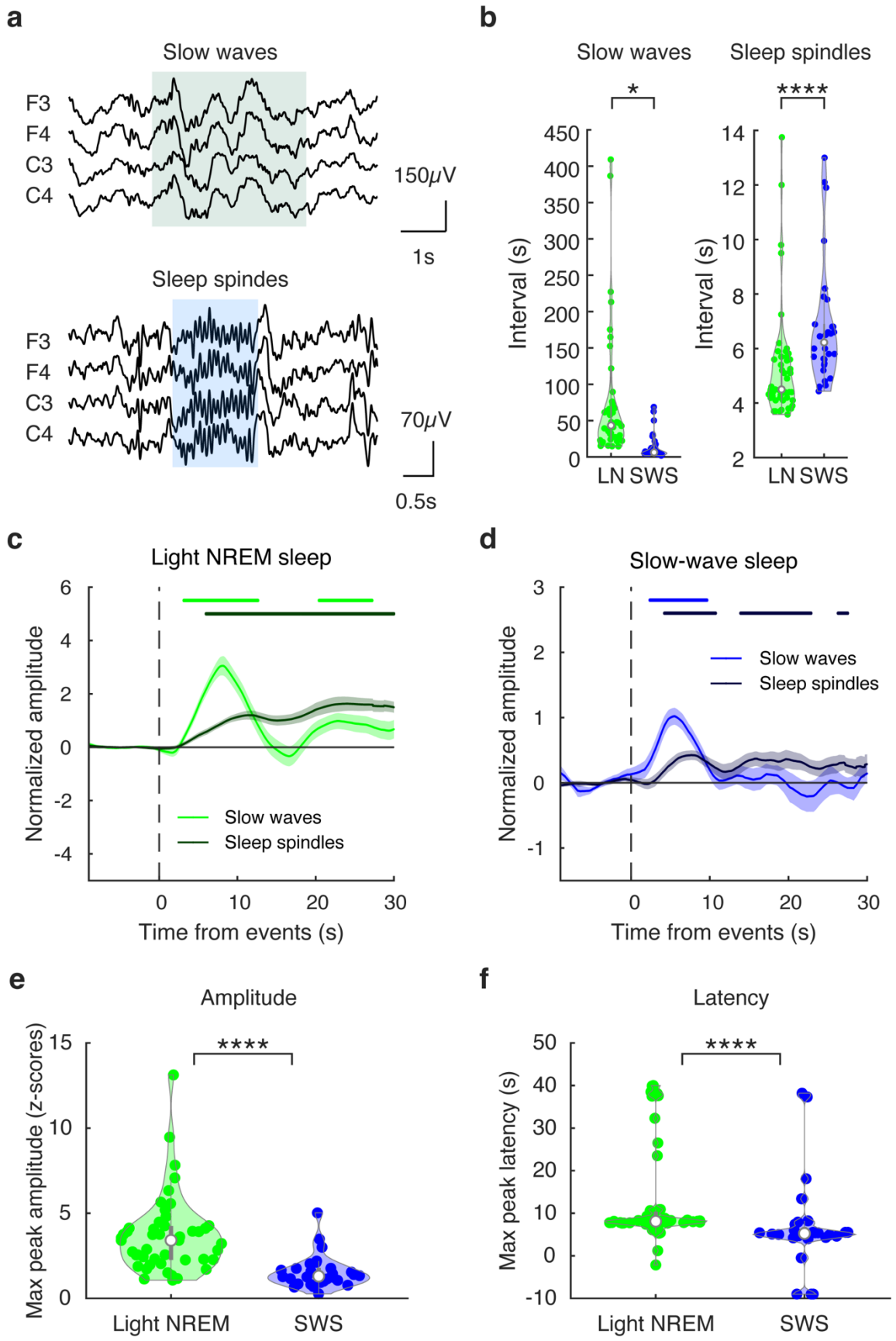
a
Slow waves
F3
F4
C3
C4
150μV
1s
Sleep spindes
F3
F4
C3
C4
70μV
0.5s
b
Slow waves
Sleep spindles
*
****
Interval (s)
LN SWS
c
Light NREM sleep
Normalized amplitude
Slow waves
Sleep spindles
Time from events (s)
d
Slow-wave sleep
Normalized amplitude
Slow waves
Sleep spindles
Time from events (s)
e
Amplitude
****
Max peak amplitude (z-scores)
Light NREM
SWS
f
Latency
****
Max peak latency (s)
Light NREM
SWS

Fig. 2: Sleep-specific brain oscillations induce faster and milder CSF dynamics during slow-wave sleep. a, Example slow waves (top) and sleep spindles (bottom) detected from the frontal and central electrodes in a representative data. **b,** Intervals of slow waves (left) and sleep spindles (right) during light NREM (green) and slow-wave sleep (blue). Two-tailed paired *t*-tests, $*P < 0.05$, $****P < 0.001$. LN, light NREM sleep. SWS, slow-wave sleep. **c,** CSF signal changes during light NREM sleep time-locked to the onset of slow waves (light green) and sleep spindles (dark green). The horizontal bars (light green, slow waves; dark green, spindles) indicate statistical significance compared with zero baselines via two-tailed one-sample *t*-tests (FDR corrected, $Ps < 0.05$). **d,** CSF signal changes during slow-wave sleep time-locked to the onset of slow waves (light blue) and sleep spindles (dark blue). The horizontal bars (light blue: slow waves; dark blue: spindles) indicate statistical significance compared with zero baselines via two-tailed one-sample *t*-tests (FDR corrected $Ps < 0.05$). **e,** Peak amplitudes of CSF signals during light NREM (green) and slow-wave sleep (blue) induced by slow waves. Two-tailed paired *t*-tests, $****P < 0.001$. SWS, slow-wave sleep. **f,** Peak latencies of CSF signals during light NREM (green) and slow-wave sleep (blue) induced by slow waves. Two-tailed paired *t*-tests, $****P < 0.001$. See **Supplementary Fig. S2** for the relationship between the CSF and GM signals. SWS, slow-wave sleep.

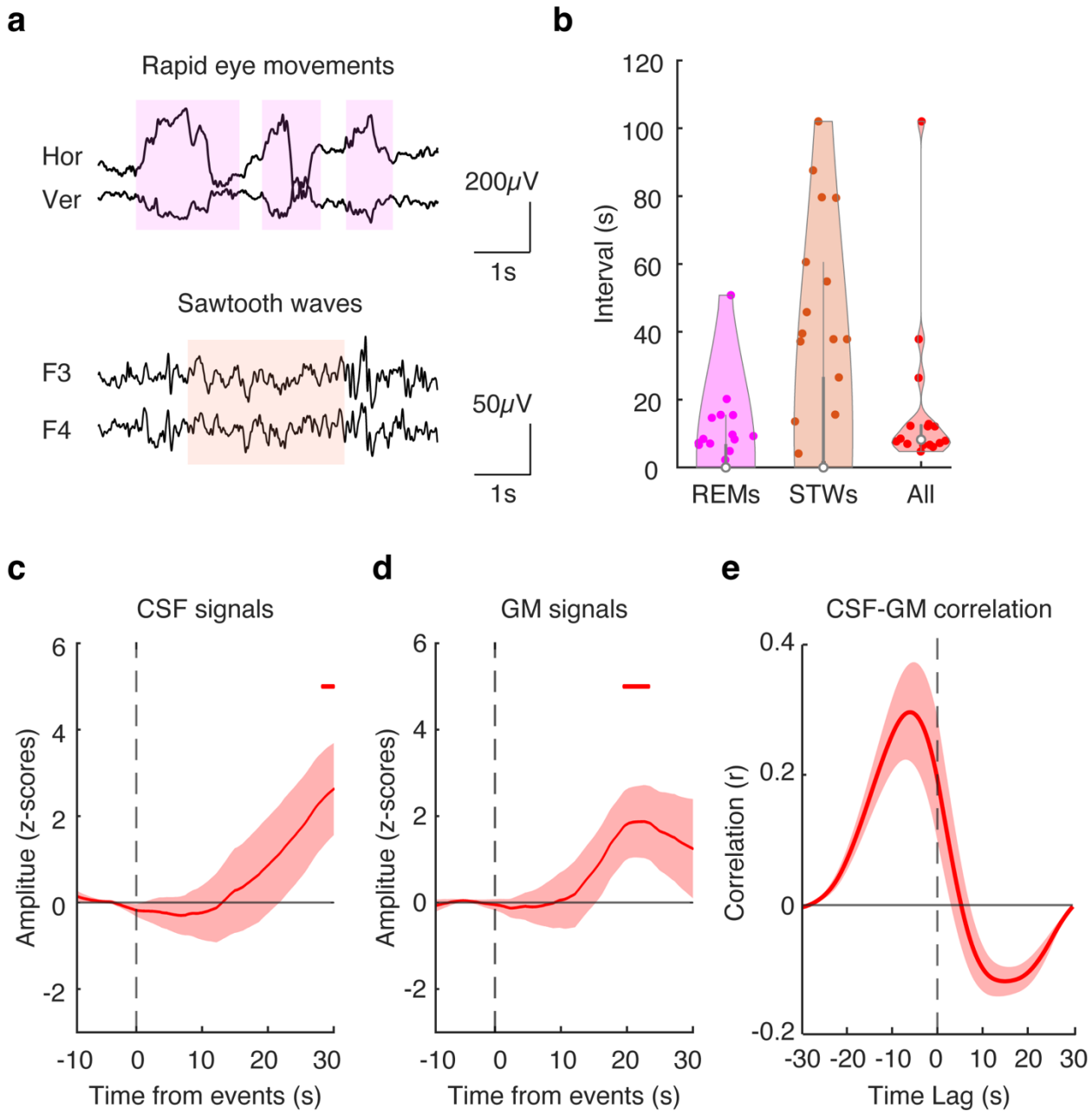

Fig. 3: REM sleep events induce changes in CSF dynamics. a, Examples of horizontal (Hor) and vertical (Ver) rapid eye movements (top) and sawtooth waves (bottom) detected from the frontal electrodes. **b,** Intervals of rapid eye movements (REMs), sawtooth waves (STWs) and all REM sleep events (All). **c,** CSF signal changes time-locked to the onset of REM sleep events. The horizontal bars represent statistical significance against zero baselines according to two-tailed one-

sample *t*-tests (FDR-corrected $P < 0.05$). **d,** GM signal changes time-locked to the onset of REM sleep events. The horizontal bars represent statistical significance against zero baselines according to two-tailed one-sample *t*-tests (FDR-corrected $P < 0.05$). **e**, Cross-correlation between CSF and GM signal changes time-locked to all REM events including rapid eye movements and sawtooth waves.

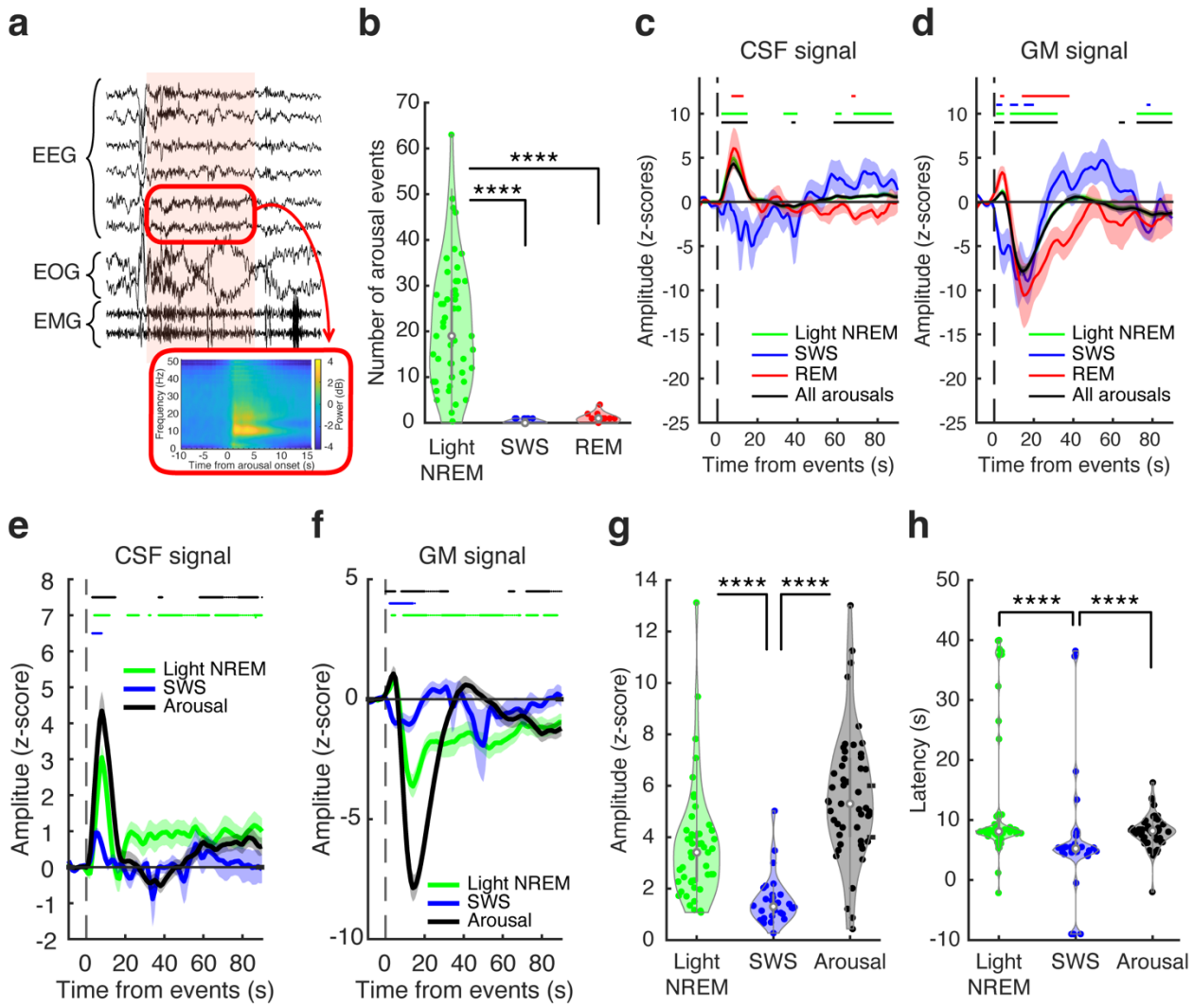

Fig. 4: Arousals induce large CSF changes during sleep. a, Example of an epoch containing an arousal event (red). The embedded diagram shows an EEG spectrogram (O1 and O2 electrodes averaged) during arousal events (number of samples = 50 sleep sessions), indicating EEG activations across a wide range of frequency bands. **b,** Number of arousals during light NREM sleep, slow-wave sleep and REM sleep stages. Two-tailed paired *t*-tests with Bonferroni correction, ****$Ps < 0.001$. **c,** CSF signal changes time-locked to arousal events for each sleep stage. The horizontal bars indicate significance against zero baselines via two-tailed one-sample *t*-tests (FDR-corrected $Ps < 0.05$). Because the majority of arousals occurred from light NREM sleep (as

indicated in **b**), the plot for light NREM sleep (light green) and that for all arousal events (black) overlap. **d,** GM signal changes time-locked to arousal events. The horizontal bars indicate significance against zero baselines via two-tailed one-sample *t*-tests (FDR-corrected *Ps* < 0.05). As in **c**, because the majority of arousals occurred from light NREM sleep, the plot for light NREM sleep (light green) and that for all arousal events (black) overlap. **e,** CSF signal changes to arousal (black), slow waves during light NREM sleep (green, same as **Fig. 2c**), and slow waves during slow-wave sleep (blue, same as **Fig. 2d**). The horizontal bars indicate significance against zero baselines via two-tailed one-sample *t*-tests (FDR-corrected *Ps* < 0.05). **f,** GM signal changes to arousal (black), slow waves during light NREM sleep (green), and slow waves during slow-wave sleep (blue). The horizontal bars indicate significance against zero baselines via two-tailed one-sample *t*-tests (FDR-corrected *Ps* < 0.05). **g,** Peak amplitudes of CSF signals induced by slow waves during light NREM sleep (green), slow-wave sleep (blue), and arousal (black). Two-tailed paired *t*-tests with Bonferroni correction, ****$Ps < 0.001$). The plots for light NREM and slow-wave sleep are the same as those in **Fig. 2e**. **h,** Mean latencies to reach the peak CSF signals induced by slow waves during light NREM sleep (green), slow-wave sleep (blue), and arousal (black). The plots for light NREM and slow-wave sleep are the same as those in **Fig. 2f**. Two-tailed paired *t*-tests with Bonferroni correction, ****$Ps < 0.001$. SWS, slow-wave sleep.

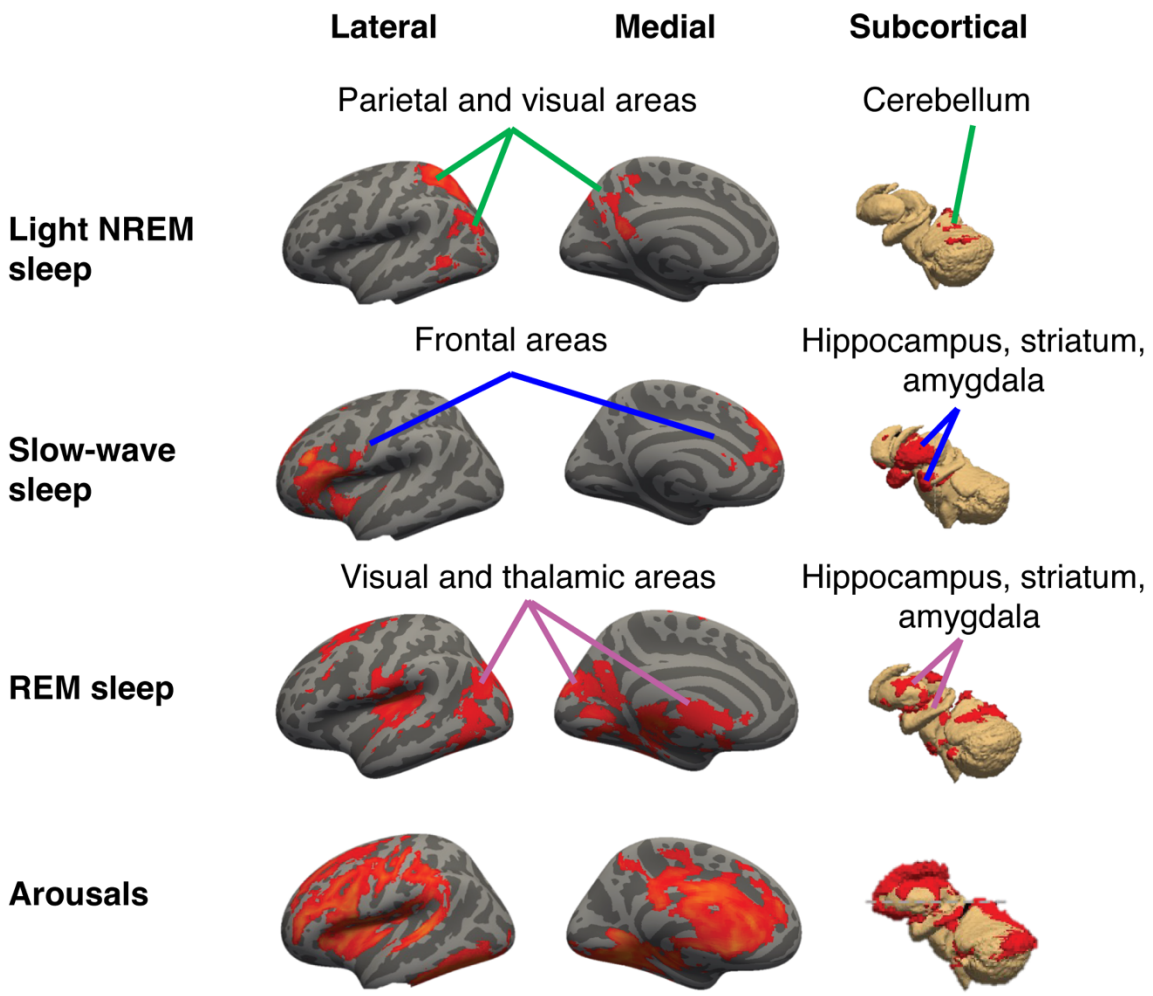

Fig. 5: Sensory and motor regions are recruited during light sleep, whereas plasticity and homeostatic circuits dominate deep sleep. A generalized linear model (GLM) analysis was performed on the MRI data corresponding to each event. A cluster-based statistical analysis was conducted at the group level, with the cluster-defining threshold ($Z > 3.1$) corrected at $P < 0.05$. Left, lateral view of the left hemisphere of a cortical surface in an inflated format. Middle, medial view of the left hemisphere of a cortical surface in an inflated format. Right, subcortical areas. The red highlighted areas in the first row indicate the areas that significantly increased during slow waves in light NREM sleep compared with those in slow-wave sleep. The red highlighted areas in the second row indicate the areas that significantly increased during slow waves in slow-wave sleep compared with those in light NREM sleep. The red highlighted areas in the third row indicate

1021 the areas that increased significantly with rapid eye movements during REM sleep. The red
1022 highlighted areas in the fourth row indicate the areas that increased significantly in response to
1023 arousals. Light NREM sleep induces sensory and motor regions, whereas slow-wave sleep induces
1024 regions involved in plasticity and homeostatic circuits. REM sleep recruits visual and plasticity
1025 circuits. Arousals accompany widespread brain activation.
1026

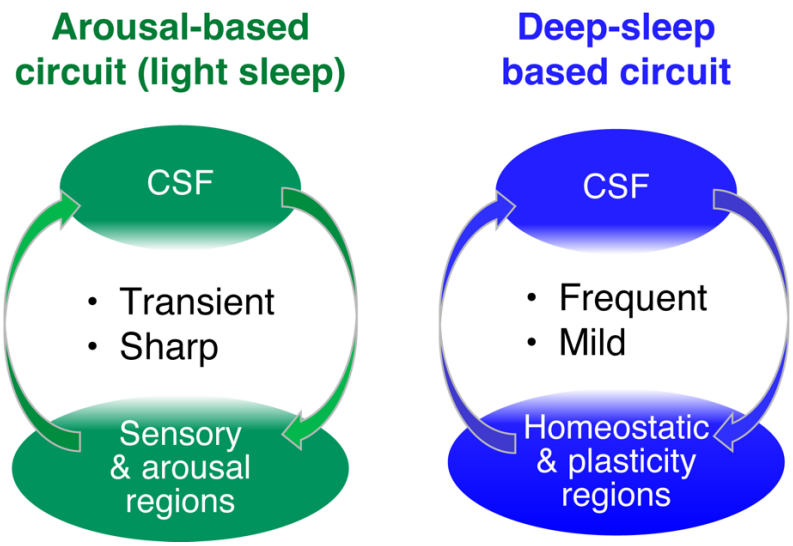

Fig. 6: An illustration of the hypothetical relationships between CSF and brain circuits during light and deep human sleep. During light sleep (left), CSF oscillations are characterized by intermittent sharp peaks induced by arousals or arousal-related waves (K-complexes). During deep sleep (right), CSF oscillations become faster, but their amplitudes are low (mild). These faster CSF oscillations are induced by sleep-related brain oscillations.

1035 ***Supplementary Note***

1036 ***The control analyses for the fourth ventricle CSF signals***

1037 Since previous research used a peak voxel inside the fourth ventricle to extract CSF signals
1038 (Fultz et al., 2019; Gonzalez-Castillo et al., 2022; Picchioni et al., 2022), in this control analysis,
1039 the same approach was applied to confirm that our findings are not limited to the lateral ventricles.
1040 However, as opposed to the previous studies (Fultz et al., 2019; Gonzalez-Castillo et al., 2022;
1041 Picchioni et al., 2022) whose MRI scan slice alignment was set up by placing the boundary edge
1042 of the imaging volume at the fourth ventricle, our MRI scan slice alignment was not optimized to
1043 the fourth ventricle CSF signals. Thus, the averaged CSF signals inside the fourth ventricle were
1044 also used to examine the CSF signal frequency profiles across different depths of sleep for this
1045 validation.

1046 The fourth ventricle was extracted as a region of interest (ROI) from each individual
1047 participant's anatomical image. The fMRI signals were motion-corrected and slice-timing
1048 corrected using AFNI (https://afni.nimh.nih.gov) and RIKEN fMRI processing programs
1049 (http://www.fmri.brain.riken.jp/~mri/Software.html). Furthermore, the fMRI data were denoised
1050 using cardiac and respiration signals (Glover et al., 2000; Hu et al., 1995). Then, the fourth
1051 ventricle ROI images were registered to each fMRI image using FSL FLIRT
1052 (https://fsl.fmrib.ox.ac.uk/fsl/fslwiki/FLIRT), and the fMRI signals were z-score transformed, and
1053 averaged across the voxels inside the ROI as the averaged fourth ventricle CSF signal for each
1054 sleep session and each participant.

1055 The location of the peak voxel inside the fourth ventricle was determined by identifying
1056 the maximum intensity of the CSF signals inside the fourth ventricle. Then, the CSF signal was
1057 extracted from the peak voxel inside the fourth ventricle and was z-score transformed for each

sleep session and each participant. Periodic oscillation components were extracted from both averaged fourth ventricle CSF signals and peak voxel CSF signals in the same way as the lateral ventricle. The same non-parametric cluster-based permutation tests were used to find significant differences ($P < 0.05$) in the periodic power spectrum across different sleep stages in both averaged fourth ventricle CSF signals and peak voxel CSF signals in the same way as the lateral ventricles.

Supplementary Table S1: Brain regions that significantly increased for slow waves during light NREM sleep than during slow-wave sleep.

ROIs	*Z* values	*P* values
Cingulate_Mid_L	3.8082	0.0002
Cingulate_Mid_R	3.6531	0.0002
Cingulate_Post_L	3.6264	0.0002
Cingulate_Post_R	3.3095	0.0006
Calcarine_L	3.7446	0.0002
Calcarine_R	3.6056	0.0003
Cuneus_L	3.7074	0.0003
Cuneus_R	3.5805	0.0003
Lingual_L	3.7504	0.0002
Lingual_R	3.7962	0.0003
Occipital_Sup_L	3.5848	0.0003
Occipital_Sup_R	3.5587	0.0003
Occipital_Mid_L	3.8243	0.0002
Occipital_Mid_R	3.6286	0.0003
Occipital_Inf_L	3.8286	0.0002
Occipital_Inf_R	3.5069	0.0004
Fusiform_L	3.5723	0.0003
Fusiform_R	3.2599	0.0006
Postcentral_L	3.7671	0.0002
Parietal_Sup_L	3.6435	0.0003
Parietal_Sup_R	3.9973	0.0002
Parietal_Inf_L	3.4056	0.0004
Parietal_Inf_R	3.3055	0.0005
Angular_L	3.4215	0.0004
Angular_R	3.4098	0.0005
Precuneus_L	4.1504	0.0001
Precuneus_R	3.7021	0.0003
Paracentral_Lobule_L	3.3912	0.0005
Temporal_Mid_L	3.5801	0.0003
Temporal_Mid_R	3.7628	0.0002
Temporal_Inf_L	3.7744	0.0002
Temporal_Inf_R	3.7552	0.0002
Cerebellum_Crus1_L	3.6657	0.0003
Cerebellum_Crus1_R	3.1931	0.0007
Cerebellum_4_5_L	3.5464	0.0003
Cerebellum_4_5_R	3.3023	0.0006
Cerebellum_6_L	3.6276	0.0001
Cerebellum_6_R	3.4245	0.0004
Vermis_4_5	3.5228	0.0003

Each ROI label is in accordance with the automated anatomical atlas 3 (Rolls et al., 2020). L, left hemisphere. R, right

hemisphere.

Supplementary Table S2: Brain regions that significantly increased for slow waves during slow-wave sleep than during light NREM sleep.

ROIs	*Z* values	*P* values
Precentral_L	3.7206	0.0003
Precentral_R	3.7044	0.0003
Frontal_Sup_2_L	3.6866	0.0003
Frontal_Sup_2_R	3.9108	0.0002
Frontal_Mid_2_L	3.3904	0.0004
Frontal_Mid_2_R	3.3258	0.0005
Frontal_Inf_Oper_L	4.3669	0.0001
Frontal_Inf_Oper_R	4.0255	0.0002
Frontal_Inf_Tri_L	4.1318	0.0002
Frontal_Inf_Tri_R	3.8356	0.0002
Frontal_Inf_Orb_2_L	4.1623	0.0001
Frontal_Inf_Orb_2_R	4.2988	0.0002
Rolandic_Oper_L	3.5048	0.0003
Rolandic_Oper_R	3.6381	0.0003
Supp_Motor_Area_L	3.9727	0.0002
Supp_Motor_Area_R	3.9846	0.0002
Olfactory_L	3.4511	0.0004
Olfactory_R	3.7452	0.0003
Frontal_Sup_Medial_L	3.9463	0.0002
Frontal_Sup_Medial_R	4.0646	0.0002
Frontal_Med_Orb_L	3.9534	0.0002
Frontal_Med_Orb_R	4.3550	0.0001
Rectus_L	3.8079	0.0003
Rectus_R	3.5458	0.0003
OFCmed_L	3.4402	0.0005
OFCmed_R	3.2660	0.0006
OFCant_L	3.4433	0.0004
OFCpost_L	3.9637	0.0002
OFCpost_R	4.0323	0.0002
OFClat_L	3.2987	0.0005
OFClat_R	3.2841	0.0005
Insula_L	4.5075	0.0001
Insula_R	4.4756	0.0001
Cingulate_Mid_L	3.6854	0.0003
Cingulate_Mid_R	3.8998	0.0002
Hippocampus_L	4.0146	0.0001
Hippocampus_R	3.7427	0.0002
ParaHippocampal_L	3.6645	0.0003
ParaHippocampal_R	3.7434	0.0002
Amygdala_L	4.0651	0.0001
Amygdala_R	3.6975	0.0002

Fusiform_L	3.5528	0.0003
Postcentral_L	3.5753	0.0003
Postcentral_R	3.8108	0.0003
Parietal_Inf_L	3.3066	0.0005
SupraMarginal_L	3.4942	0.0004
SupraMarginal_R	3.8776	0.0002
Paracentral_Lobule_L	3.4346	0.0004
Caudate_L	3.5091	0.0003
Caudate_R	3.4317	0.0004
Putamen_L	3.6246	0.0003
Putamen_R	3.7300	0.0003
Pallidum_L	3.2837	0.0006
Temporal_Sup_L	3.5406	0.0003
Temporal_Pole_Sup_L	3.7996	0.0002
Temporal_Pole_Sup_R	3.7752	0.0002
Temporal_Pole_Mid_L	3.4469	0.0004
ACC_sub_L	3.6190	0.0003
ACC_sub_R	3.6659	0.0002
ACC_pre_L	4.2652	0.0001
ACC_pre_R	4.4827	0.0001
ACC_sup_L	3.6695	0.0003
ACC_sup_R	3.9976	0.0002
N_Acc_L	3.5404	0.0003
N_Acc_R	3.5088	0.0003

Each ROI label is in accordance with the automated anatomical atlas 3 (Rolls et al., 2020). L, left hemisphere. R, right hemisphere.

Supplementary Table S3: Brain regions that significantly increased for rapid eye movements during REM sleep.

ROIs	*Z* values	*P* values
Supp_Motor_Area_L	3.2030	0.0007
Hippocampus_L	3.4546	0.0004
Hippocampus_R	3.7187	0.0002
ParaHippocampal_L	3.3809	0.0004
ParaHippocampal_R	3.9307	0.0002
Calcarine_L	3.3290	0.0005
Calcarine_R	3.4544	0.0004
Lingual_L	3.3523	0.0005
Lingual_R	3.4621	0.0004
Occipital_Sup_L	3.2501	0.0006
Cerebellum_3_L	3.2661	0.0006
Cerebellum_3_R	3.1315	0.0009
Cerebellum_4_5_L	3.6211	0.0002
Cerebellum_4_5_R	3.3396	0.0005
Cerebellum_6_L	3.2634	0.0006
Cerebellum_6_R	3.3340	0.0005
Cerebellum_9_L	3.1488	0.0008
Vermis_1_2	3.2139	0.0007
Vermis_3	3.5091	0.0004
Vermis_4_5	3.4872	0.0004
Vermis_6	3.3777	0.0005
Vermis_10	3.1045	0.0010
Thal_VA_L	3.3155	0.0005
Thal_VA_R	3.2629	0.0006
Thal_VL_L	3.6201	0.0003
Thal_VL_R	3.6587	0.0003
Thal_VPL_L	3.5085	0.0004
Thal_VPL_R	3.5499	0.0003
Thal_IL_L	3.9072	0.0002
Thal_IL_R	4.2275	0.0000
Thal_MDm_L	3.8869	0.0002
Thal_MDm_R	3.7111	0.0003
Thal_MDl_L	4.0575	0.0001
Thal_MDl_R	3.7768	0.0002
Thal_LGN_L	3.3645	0.0004
Thal_LGN_R	3.2806	0.0006
Thal_MGN_L	3.3011	0.0005
Thal_MGN_R	3.5171	0.0003
Thal_PuI_L	3.2652	0.0006
Thal_PuI_R	3.2704	0.0006
Thal_PuM_L	3.4233	0.0004
Thal_PuM_R	3.5812	0.0003

Thal_PuA_L	3.6875	0.0002
Thal_PuA_R	3.7081	0.0002
Thal_PuL_L	3.2427	0.0006
Thal_PuL_R	3.3158	0.0005
VTA_R	3.1182	0.0009
SN_pc_L	3.1993	0.0007
SN_pc_R	3.4885	0.0004
SN_pr_L	3.2564	0.0006
SN_pr_R	3.4536	0.0004
Red_N_L	3.4694	0.0003
Red_N_R	3.6793	0.0002
Raphe_D	3.4396	0.0004

Each ROI label is in accordance with the automated anatomical atlas 3 (Rolls et al., 2020). L, left hemisphere. R, right hemisphere.

Supplementary Table S4: Brain regions that significantly increased for arousals.

ROIs	*Z* values	*P* values
Frontal_Sup_2_R	3.6E+00	3.4E-04
Frontal_Mid_2_L	3.7E+00	3.5E-04
Frontal_Mid_2_R	3.6E+00	2.7E-04
Frontal_Inf_Oper_L	3.7E+00	2.4E-04
Frontal_Inf_Oper_R	3.6E+00	1.9E-04
Frontal_Inf_Orb_2_L	4.3E+00	8.3E-05
Frontal_Inf_Orb_2_R	4.3E+00	1.5E-04
Rolandic_Oper_L	3.2E+00	6.8E-04
Rolandic_Oper_R	3.3E+00	5.0E-04
Supp_Motor_Area_L	3.8E+00	2.2E-04
Supp_Motor_Area_R	3.6E+00	2.8E-04
Olfactory_L	3.9E+00	1.9E-04
Olfactory_R	4.0E+00	1.7E-04
Frontal_Sup_Medial_L	3.5E+00	3.4E-04
Frontal_Med_Orb_R	3.8E+00	6.8E-05
Rectus_L	3.9E+00	1.5E-04
Rectus_R	4.0E+00	1.8E-04
OFCmed_L	3.4E+00	3.9E-04
OFCmed_R	3.5E+00	3.0E-04
OFCant_L	3.9E+00	1.5E-04
OFCant_R	4.0E+00	1.6E-04
OFCpost_L	3.6E+00	3.9E-04
OFCpost_R	3.7E+00	9.3E-05
Insula_L	3.9E+00	2.1E-04
Insula_R	3.7E+00	2.5E-04
Cingulate_Mid_L	3.9E+00	2.0E-04
Cingulate_Mid_R	3.9E+00	2.0E-04
Cingulate_Post_L	4.3E+00	9.7E-05
Cingulate_Post_R	4.0E+00	1.4E-04
Hippocampus_L	4.1E+00	1.4E-04
Hippocampus_R	4.4E+00	1.0E-04
ParaHippocampal_L	4.0E+00	1.9E-04
ParaHippocampal_R	4.3E+00	1.2E-04
Amygdala_L	4.2E+00	1.1E-04
Amygdala_R	5.0E+00	3.1E-05
Calcarine_R	3.7E+00	2.0E-04
Cuneus_R	3.8E+00	1.7E-04
Lingual_L	3.7E+00	2.7E-04
Lingual_R	4.1E+00	1.3E-04
Occipital_Sup_L	3.6E+00	2.5E-04
Occipital_Sup_R	3.2E+00	7.4E-04
Occipital_Inf_L	3.7E+00	2.1E-04

Fusiform_L	3.8E+00	2.2E-04
Fusiform_R	4.3E+00	1.2E-04
Parietal_Sup_L	3.5E+00	3.7E-04
Parietal_Inf_L	3.4E+00	2.8E-04
SupraMarginal_R	3.1E+00	9.2E-04
Angular_L	3.3E+00	5.1E-04
Precuneus_L	3.6E+00	3.1E-04
Precuneus_R	3.7E+00	2.7E-04
Paracentral_Lobule_L	3.8E+00	2.5E-04
Paracentral_Lobule_R	3.7E+00	3.0E-04
Caudate_L	4.6E+00	8.3E-05
Caudate_R	5.1E+00	2.1E-05
Putamen_L	4.9E+00	3.9E-05
Putamen_R	4.9E+00	4.3E-05
Pallidum_L	4.7E+00	7.7E-05
Pallidum_R	4.6E+00	3.0E-05
Heschl_R	3.3E+00	5.8E-04
Temporal_Sup_L	3.4E+00	4.4E-04
Temporal_Sup_R	3.6E+00	3.7E-04
Temporal_Pole_Sup_L	3.3E+00	5.8E-04
Temporal_Pole_Sup_R	3.5E+00	3.3E-04
Temporal_Mid_L	3.5E+00	4.4E-04
Temporal_Mid_R	3.4E+00	3.5E-04
Temporal_Inf_L	3.9E+00	2.4E-04
Temporal_Inf_R	3.8E+00	2.4E-04
Cerebellum_Crus1_L	4.7E+00	6.1E-05
Cerebellum_Crus1_R	4.3E+00	1.2E-04
Cerebellum_Crus2_L	4.0E+00	1.8E-04
Cerebellum_Crus2_R	4.1E+00	1.4E-04
Cerebellum_3_L	4.6E+00	6.3E-05
Cerebellum_3_R	4.4E+00	9.7E-05
Cerebellum_4_5_L	4.7E+00	6.0E-05
Cerebellum_4_5_R	4.8E+00	5.6E-05
Cerebellum_6_L	4.7E+00	6.7E-05
Cerebellum_6_R	4.7E+00	6.1E-05
Cerebellum_7b_L	3.6E+00	2.8E-04
Cerebellum_8_L	3.7E+00	2.6E-04
Cerebellum_8_R	3.7E+00	2.9E-04
Cerebellum_9_L	3.7E+00	2.4E-04
Cerebellum_9_R	3.5E+00	3.6E-04
Cerebellum_10_L	3.6E+00	3.6E-04
Cerebellum_10_R	3.7E+00	2.0E-04
Vermis_1_2	4.2E+00	8.7E-05
Vermis_3	4.0E+00	1.4E-04
Vermis_4_5	5.3E+00	1.7E-05

Vermis_6	5.6E+00	8.2E-06
Vermis_7	4.8E+00	1.2E-05
Vermis_8	4.7E+00	7.9E-05
Vermis_9	4.1E+00	1.2E-04
Vermis_10	3.5E+00	3.5E-04
Thal_AV_L	5.6E+00	7.0E-06
Thal_AV_R	5.1E+00	5.5E-05
Thal_LP_L	3.8E+00	2.0E-04
Thal_LP_R	3.7E+00	2.4E-04
Thal_VA_L	5.6E+00	2.8E-07
Thal_VA_R	5.9E+00	1.4E-06
Thal_VL_L	5.3E+00	7.3E-06
Thal_VL_R	5.6E+00	1.0E-05
Thal_VPL_L	4.5E+00	7.5E-05
Thal_VPL_R	4.6E+00	7.5E-05
Thal_IL_L	4.6E+00	5.1E-05
Thal_IL_R	4.7E+00	1.8E-05
Thal_Re_L	5.2E+00	6.4E-07
Thal_Re_R	5.3E+00	5.5E-08
Thal_MDm_L	5.7E+00	1.6E-06
Thal_MDm_R	5.6E+00	1.5E-06
Thal_MDl_L	5.6E+00	3.2E-07
Thal_MDl_R	5.3E+00	1.3E-07
Thal_LGN_L	3.2E+00	6.3E-04
Thal_LGN_R	3.9E+00	1.3E-04
Thal_MGN_L	3.3E+00	5.1E-04
Thal_MGN_R	3.6E+00	3.1E-04
Thal_PuI_L	3.5E+00	2.3E-04
Thal_PuM_L	4.0E+00	1.5E-04
Thal_PuM_R	4.4E+00	1.1E-04
Thal_PuA_L	4.4E+00	4.6E-05
Thal_PuA_R	4.2E+00	8.6E-05
Thal_PuL_L	4.1E+00	1.0E-04
Thal_PuL_R	3.8E+00	2.1E-04
ACC_sub_L	3.7E+00	3.8E-04
ACC_sub_R	3.8E+00	1.9E-04
ACC_pre_L	3.5E+00	3.4E-04
ACC_pre_R	3.6E+00	2.9E-04
ACC_sup_L	4.5E+00	7.4E-05
ACC_sup_R	4.1E+00	1.4E-04
N_Acc_L	4.7E+00	6.6E-05
N_Acc_R	5.0E+00	2.2E-05
VTA_L	5.4E+00	1.2E-06
VTA_R	5.0E+00	1.9E-06
SN_pc_L	4.8E+00	4.4E-05

SN_pc_R	4.9E+00	4.9E-06
SN_pr_L	4.3E+00	7.6E-05
SN_pr_R	4.8E+00	3.1E-05
Red_N_L	4.1E+00	1.7E-04
Red_N_R	3.9E+00	1.8E-04
LC_L	4.2E+00	6.4E-05
LC_R	4.0E+00	2.8E-04
Raphe_D	4.5E+00	7.5E-05
Raphe_M	4.6E+00	1.3E-05

Each ROI label is in accordance with the automated anatomical atlas 3 (Rolls et al., 2020). L, left hemisphere. R, right hemisphere.

Supplementary Table S5: Brain regions that increased significantly for sleep spindles during light NREM sleep than during slow-wave sleep.

ROIs	*Z* values	*P* values
Precentral_L	3.4296	0.0004
Precentral_R	3.4019	0.0004
Frontal_Sup_2_R	3.1556	0.0008
Frontal_Mid_2_R	3.1447	0.0008
Frontal_Inf_Oper_L	3.4841	0.0005
Rolandic_Oper_L	3.6361	0.0003
Rolandic_Oper_R	3.4432	0.0004
Supp_Motor_Area_L	3.4196	0.0004
Supp_Motor_Area_R	3.3864	0.0004
Frontal_Sup_Medial_L	3.2095	0.0007
Insula_L	3.5361	0.0003
Insula_R	3.6424	0.0003
Cingulate_Mid_L	3.4839	0.0003
Cingulate_Mid_R	3.5164	0.0003
Postcentral_L	3.4082	0.0004
Postcentral_R	3.3369	0.0005
SupraMarginal_L	3.3497	0.0005
SupraMarginal_R	3.3474	0.0004
Precuneus_L	3.2277	0.0007
Precuneus_R	3.2651	0.0006
Paracentral_Lobule_L	3.3886	0.0004
Paracentral_Lobule_R	3.4239	0.0004
Putamen_R	3.5491	0.0003
Heschl_L	3.7458	0.0002
Heschl_R	3.7344	0.0002
Temporal_Sup_L	3.6067	0.0003
Temporal_Sup_R	3.5031	0.0003
Temporal_Pole_Sup_L	3.5521	0.0003
Temporal_Pole_Sup_R	3.3365	0.0005
Temporal_Mid_L	3.4501	0.0004
Temporal_Mid_R	3.1425	0.0008
ACC_sup_L	3.3683	0.0004
ACC_sup_R	3.2987	0.0005

Each ROI label is in accordance with the automated anatomical atlas 3 (Rolls et al., 2020). L, left hemisphere. R, right hemisphere.

Supplementary Table S6: Brain regions that increased significantly for sleep spindles during slow-wave sleep than during light NREM sleep.

ROIs	*Z* values	*P* values
ParaHippocampal_R	3.2843	0.0005
Calcarine_R	3.7146	0.0003
Cuneus_L	3.3800	0.0005
Cuneus_R	3.5743	0.0003
Lingual_R	3.2666	0.0006
Occipital_Sup_L	3.2750	0.0006
Fusiform_R	3.2916	0.0006
Parietal_Sup_L	3.3117	0.0005
Parietal_Sup_R	3.2652	0.0006
Precuneus_L	3.2913	0.0006
Precuneus_R	3.7949	0.0002
Cerebellum_Crus1_R	3.2078	0.0007
Cerebellum_3_R	3.2160	0.0007
Cerebellum_4_5_R	3.3673	0.0005
Cerebellum_6_R	3.3231	0.0005

Each ROI label is in accordance with the automated anatomical atlas 3 (Rolls et al., 2020). L, left hemisphere. R, right hemisphere.

Supplementary Table S7: Brain regions that increased significantly for sawtooth waves during REM sleep.

ROIs	*Z* values	*P* values
Frontal_Inf_Oper_R	3.2735	0.0005
Calcarine_L	3.2675	0.0006
Lingual_L	3.2436	0.0006
Paracentral_Lobule_R	3.1408	0.0008
Heschl_L	3.1726	0.0008
Vermis_9	3.2986	0.0005
Thal_VPL_L	3.1857	0.0007
Thal_PuM_L	3.2213	0.0007
Thal_PuL_L	3.2732	0.0005

Each ROI label is in accordance with the automated anatomical atlas 3 (Rolls et al., 2020). L, left hemisphere. R, right hemisphere.

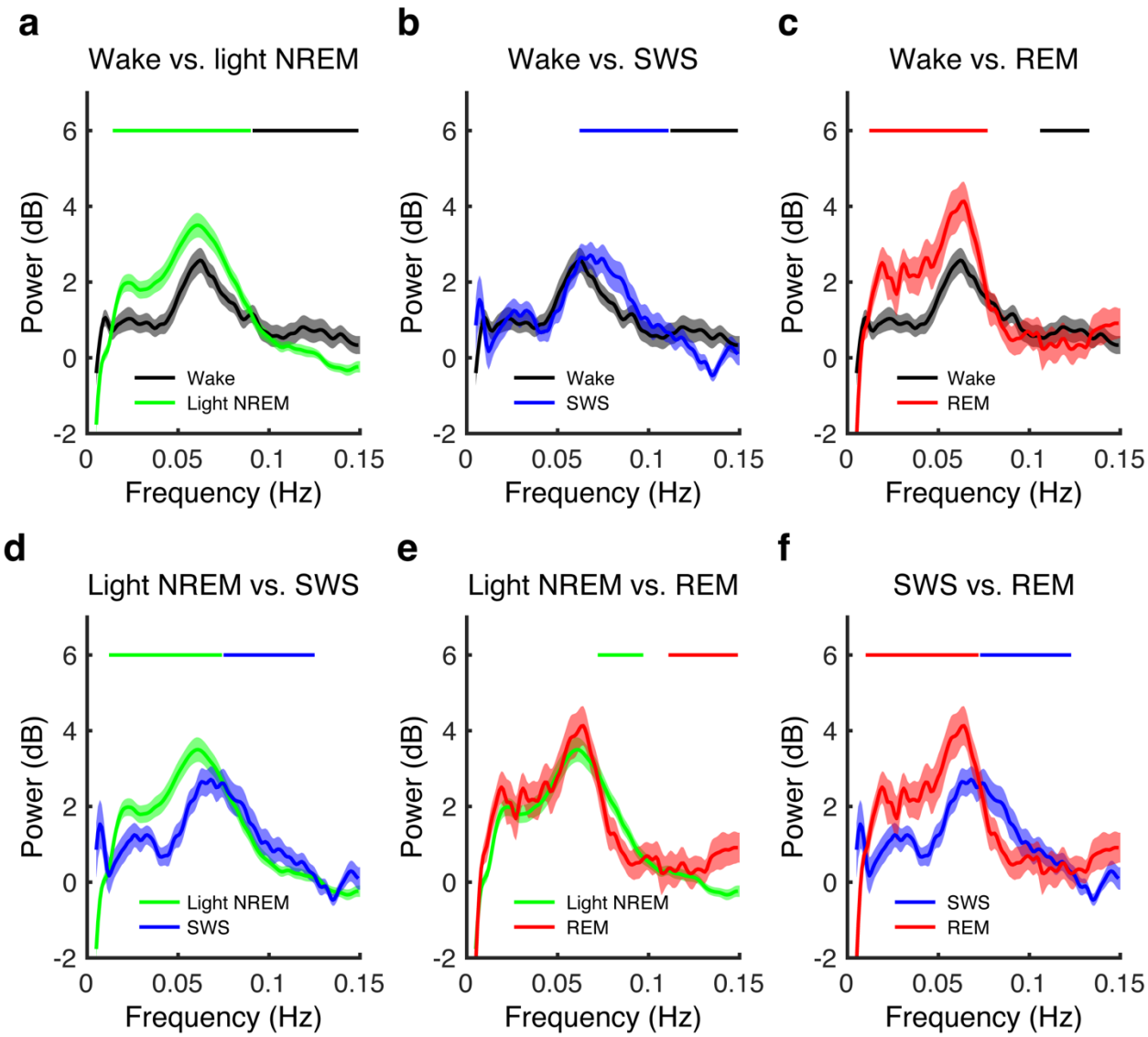

Supplementary Fig. S1: Comparisons of periodic CSF signal power spectrum against each frequency bin across different sleep depths. a, Wakefulness vs. light NREM sleep. **b**, Wakefulness vs. slow-wave sleep. **c**, Wakefulness vs. REM sleep. **d**, Light NREM sleep vs. slow-wave sleep. **e**, Light NREM sleep vs. REM sleep. **f**, Slow-wave sleep vs. REM sleep. Cluster-based permutation results for possible pairs were conducted. The horizontal bars represent a significant cluster (horizontal bars, cluster-based permutation tests, $Ps < 0.05$). SWS, slow-wave sleep.

1212

1213

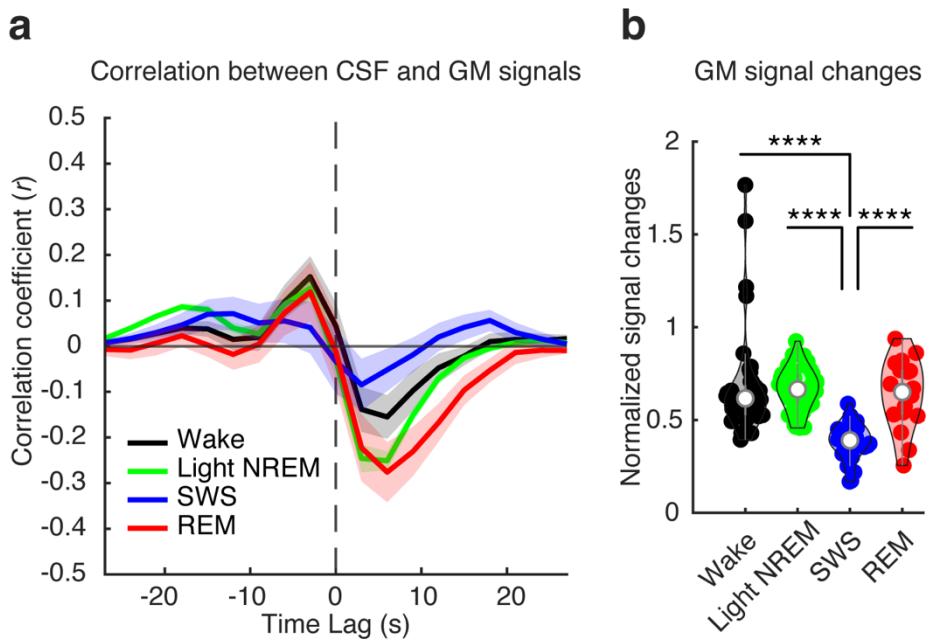

Supplementary Fig. S2: Relationship between CSF and GM signal. a, Cross-correlation between CSF and GM signals. CSF and GM signals were generally anti-correlated. **b**, GM signal variances during different sleep stages. GM signal changes were significantly smaller during slow-wave sleep than during wakefulness (P = 3.2017e-05), light NREM sleep (P < 1e-10) or REM sleep (P = 1.9815e-06). SWS, slow-wave sleep. Two-tailed paired t-test with Bonferroni correction, ****P < 0.001

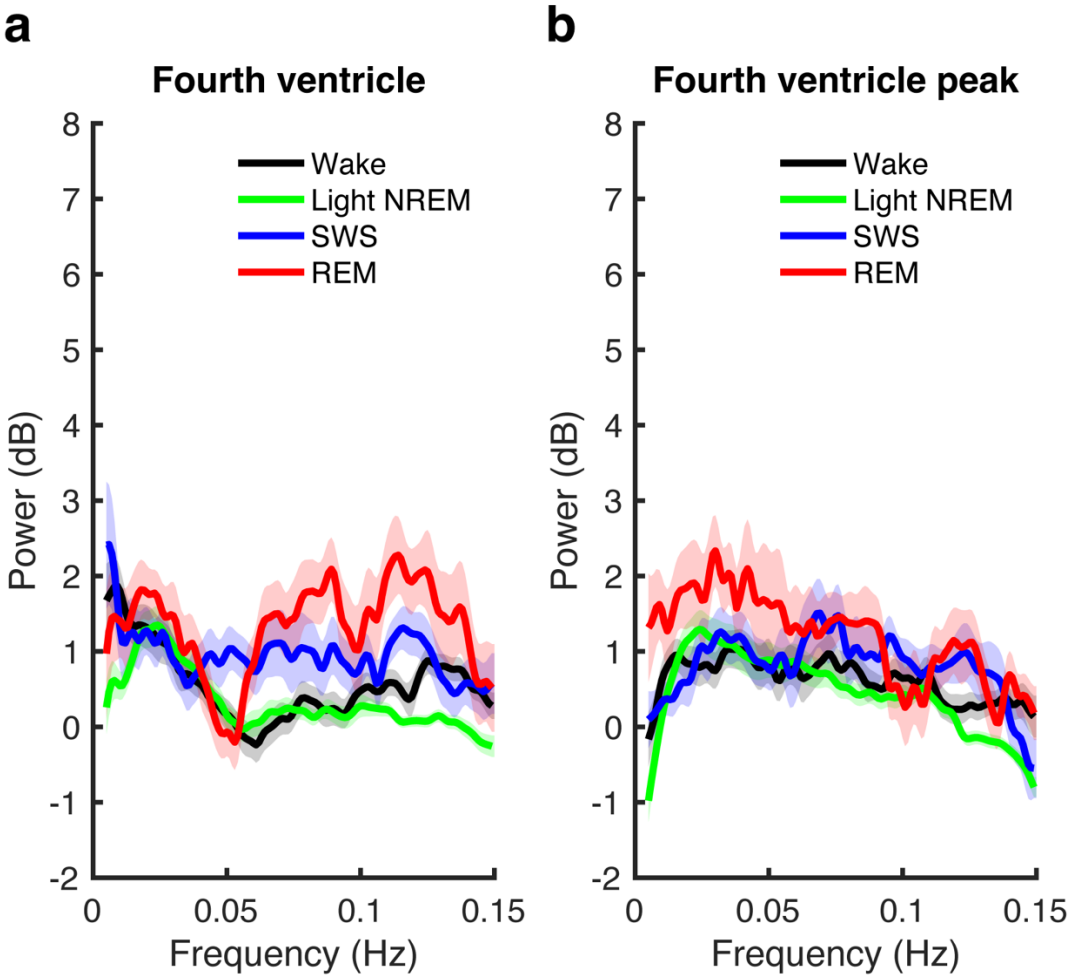

Supplementary Fig. S3: Periodic CSF frequency profiles obtained from the fourth ventricles (a) and the peak voxel of the fourth ventricles (b). SWS, slow-wave sleep. See ***Supplementary Note*** for more details.

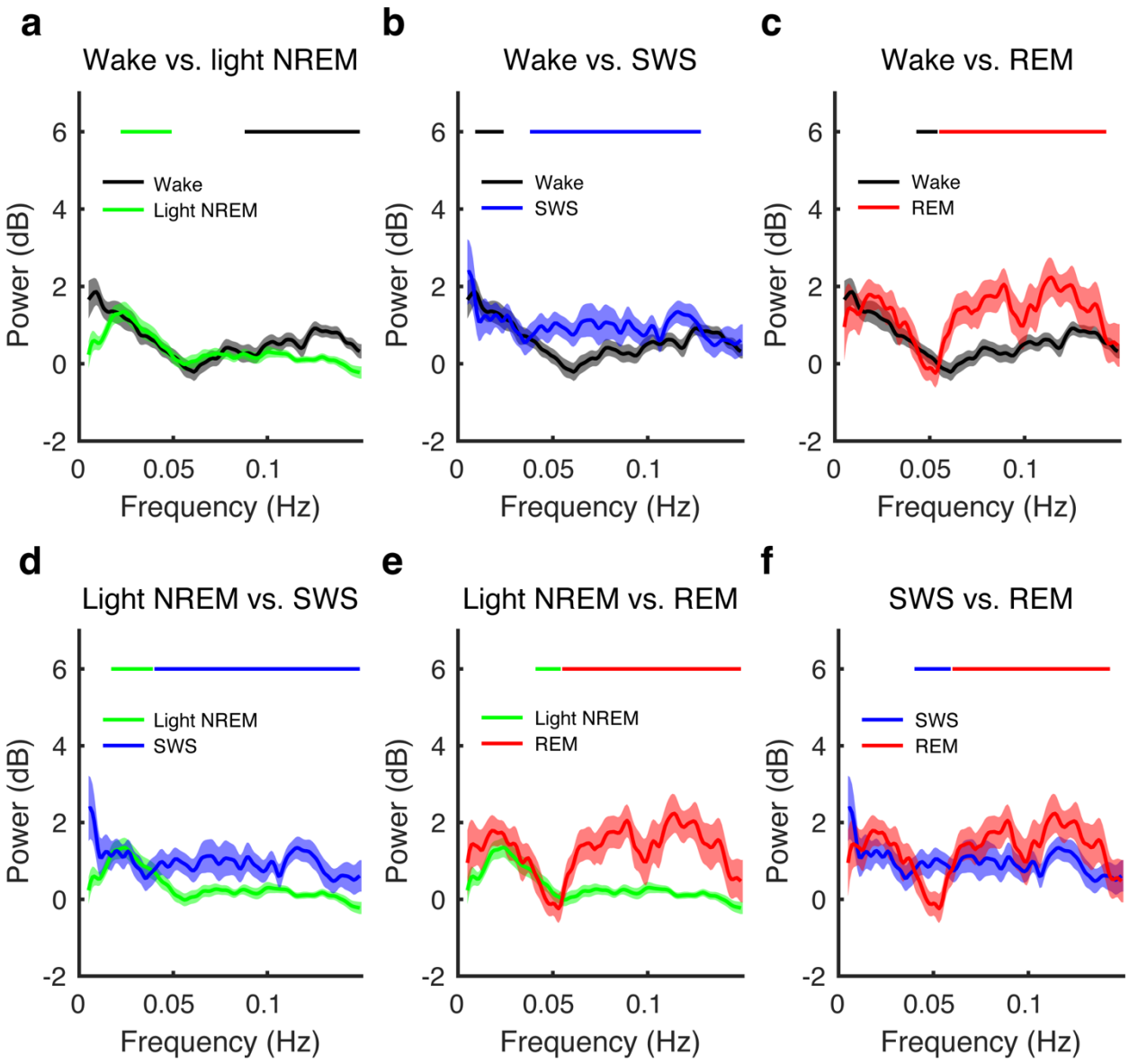

Supplementary Fig. S4: CSF signals obtained from the fourth ventricles. Comparisons of the spectrum against each frequency bin across different sleep depths. **a**, Wakefulness vs. light NREM sleep. **b**, Wakefulness vs. slow-wave sleep. **c**, Wakefulness vs. REM sleep. **d**, Light NREM sleep vs. slow-wave sleep. **e**, Light NREM sleep vs. REM sleep. **f**, Slow-wave sleep vs. REM sleep. Cluster-based permutation results for possible pairs were conducted. The horizontal

1238 bars represent a significant cluster (horizontal bars, cluster-based permutation tests, $Ps < 0.05$).

1239 SWS, slow-wave sleep.

1240

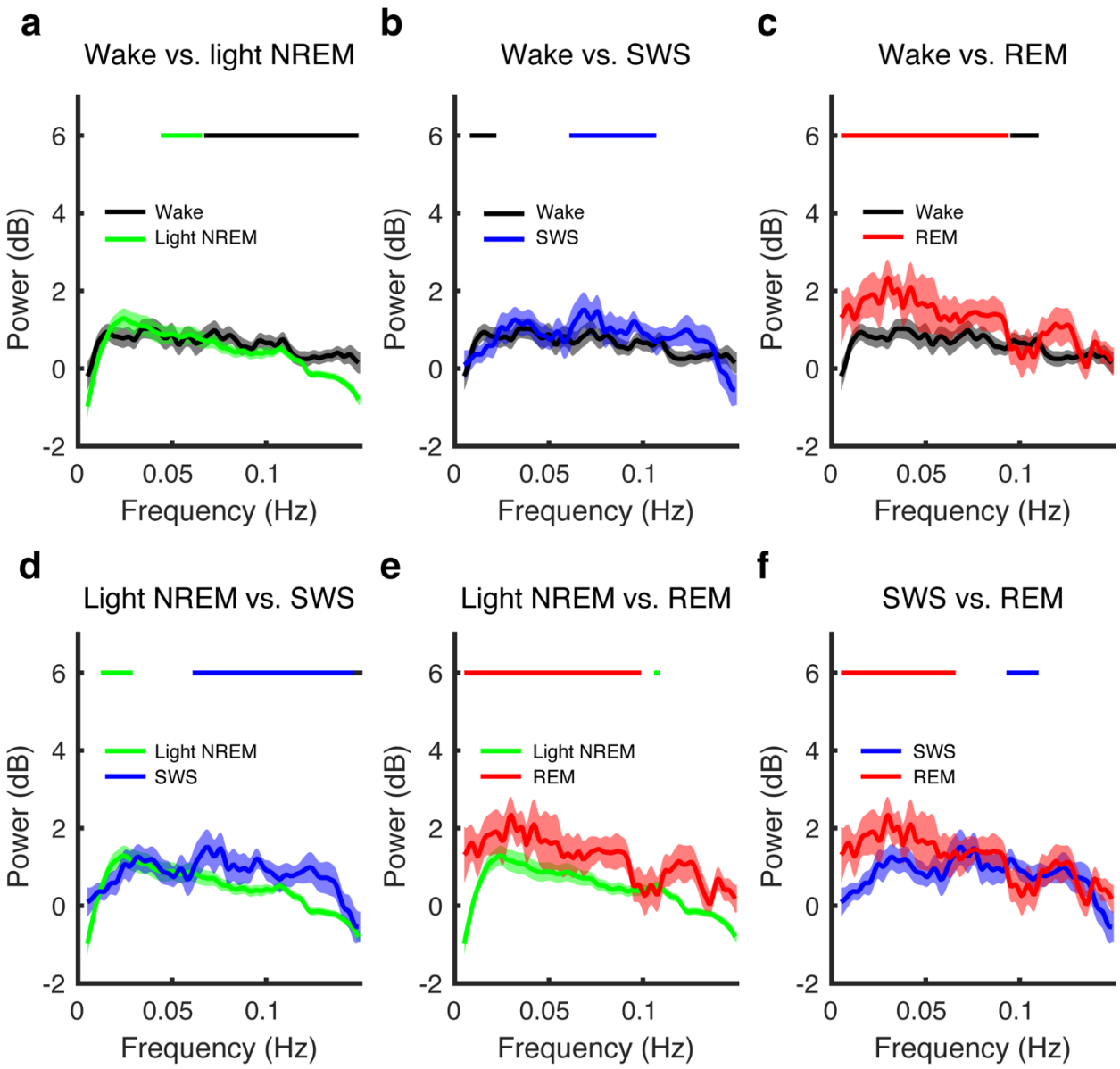

Supplementary Fig. S5: CSF signals obtained from the peak voxel in the fourth ventricles. Comparisons of the spectrum against each frequency bin across different sleep depths. **a**, Wakefulness vs. light NREM sleep. **b**, Wakefulness vs. slow-wave sleep. **c**, Wakefulness vs. REM sleep. **d**, Light NREM sleep vs. slow-wave sleep. **e**, Light NREM sleep vs. REM sleep. **f**, Slow-wave sleep vs. REM sleep. Cluster-based permutation results for possible pairs were

1248 conducted. The horizontal bars represent a significant cluster (horizontal bars, cluster-based

1249 permutation tests, $Ps < 0.05$). SWS, slow-wave sleep.

1250

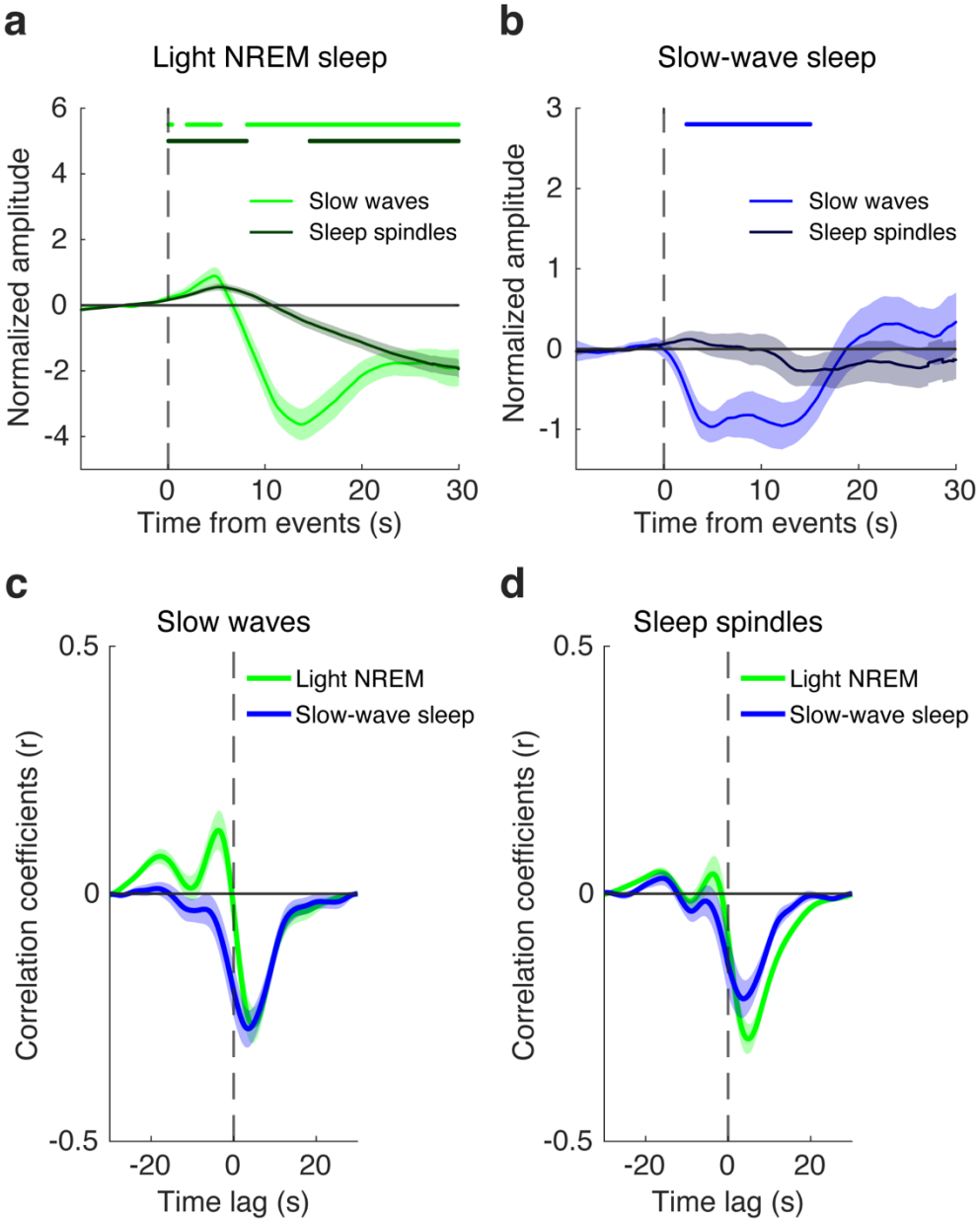

Supplementary Fig. S6: GM signal changes time-locked to slow waves and sleep spindles. a, GM signal amplitude changes time-locked to slow waves (light green) and sleep spindles (dark green) during light NREM sleep. The horizontal bars (light green: slow waves; dark green, sleep spindles) indicate significances against zero baselines using two-tailed one-sample t-tests, (FDR corrected, *Ps* < 0.05). **b**, GM signal amplitude changes time-locked to slow waves (light blue)

1258 and sleep spindles (dark blue) during slow-wave sleep. The horizontal bar (light blue, slow
1259 waves) indicates significances against zero baselines using two-tailed one-sample t-tests, (FDR
1260 corrected, *Ps* < 0.05). **c**, Cross-correlation between CSF and GM signals time-locked to slow
1261 waves. Green, light NREM sleep. Blue, slow-waves sleep. **d**, Cross-correlation between CSF and
1262 GM signals time-locked to sleep spindles. Green, light NREM sleep. Blue, slow-waves sleep.

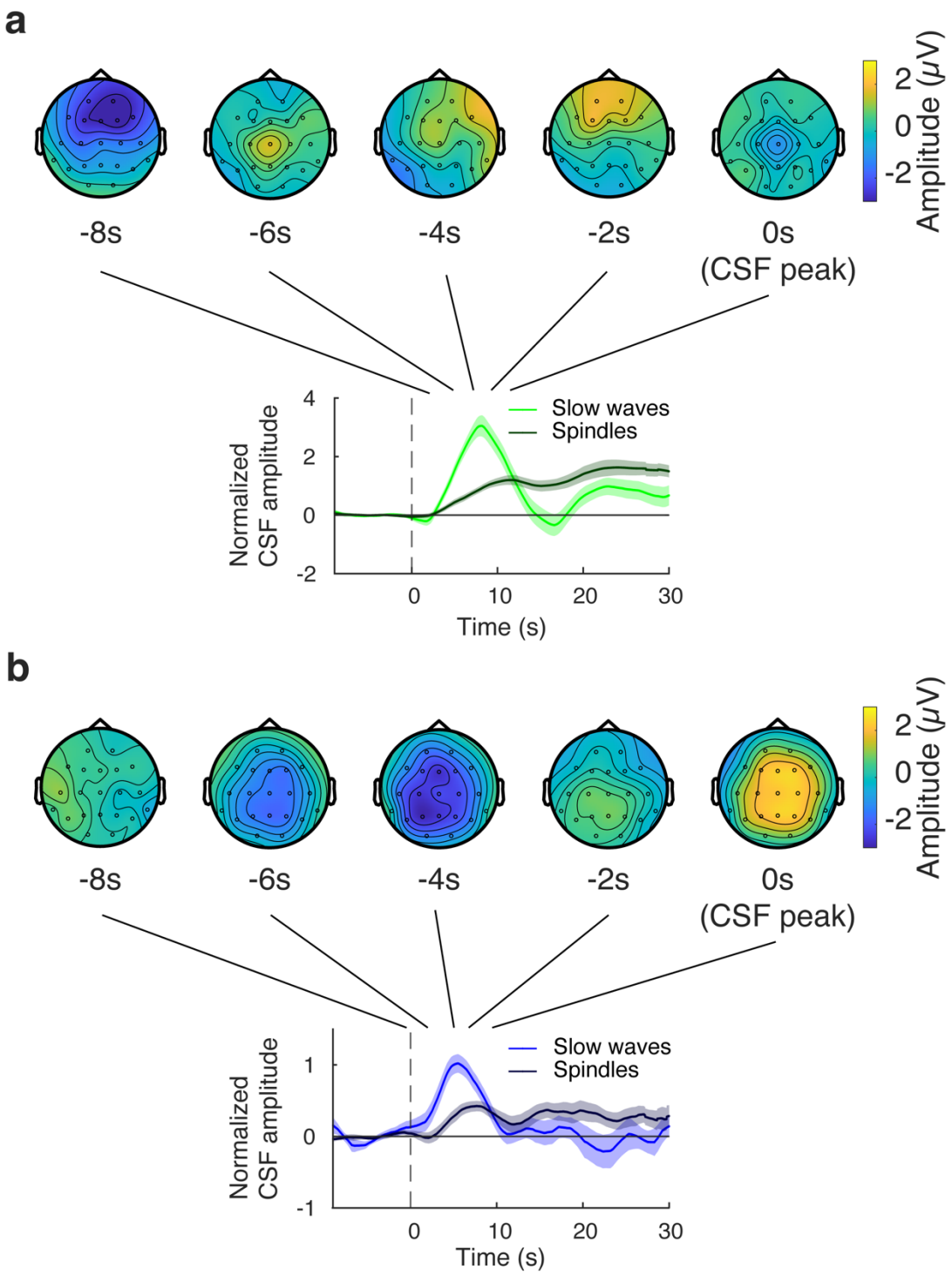

Supplementary Fig. S7: EEG topographical changes time-locked to CSF signal peaks during light NREM (a) and slow-wave sleep (b). t=0s corresponds to the CSF signal peak.

EEG topographic map indicated a negative peak centered around the frontal region, resembling a topography of K-complexes, which peaked 8 s *before* the CSF positive peak events during light NREM sleep. A negative peak spread through the midline of frontal to parietal regions resembling those found typically in slow waves (Adamantidis et al., 2019) which peaked around 5 s *before* the CSF positive peak events during slow-wave sleep. Note that slow waves during slow-wave sleep were followed by a CSF peak 5.5s *after* the onset of the events. The plots for CSF signals are the same as those in **Fig. 2c** and **d**.

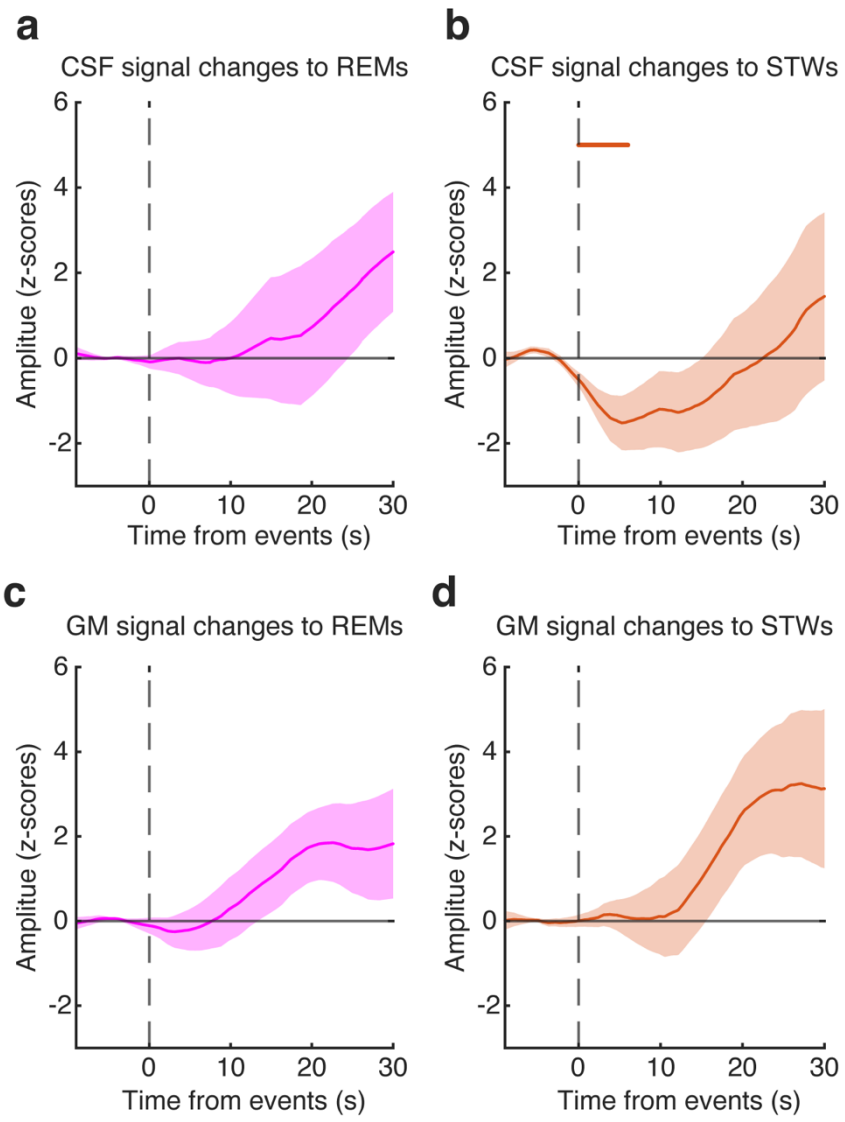

Supplementary Fig. S8: CSF and GM signal changes time-locked to events during REM sleep. a, CSF signal changes to rapid eye movements (REMs). **b**, CSF signal changes to sawtooth waves (STWs). The horizontal bar (orange, sawtooth waves) indicates significances against zero baselines using two-tailed one-sample t-tests, (FDR corrected, *Ps* < 0.05). **c**, GM signal changes to rapid eye movements (REMs). **d**, GM signal changes to sawtooth waves (STWs).

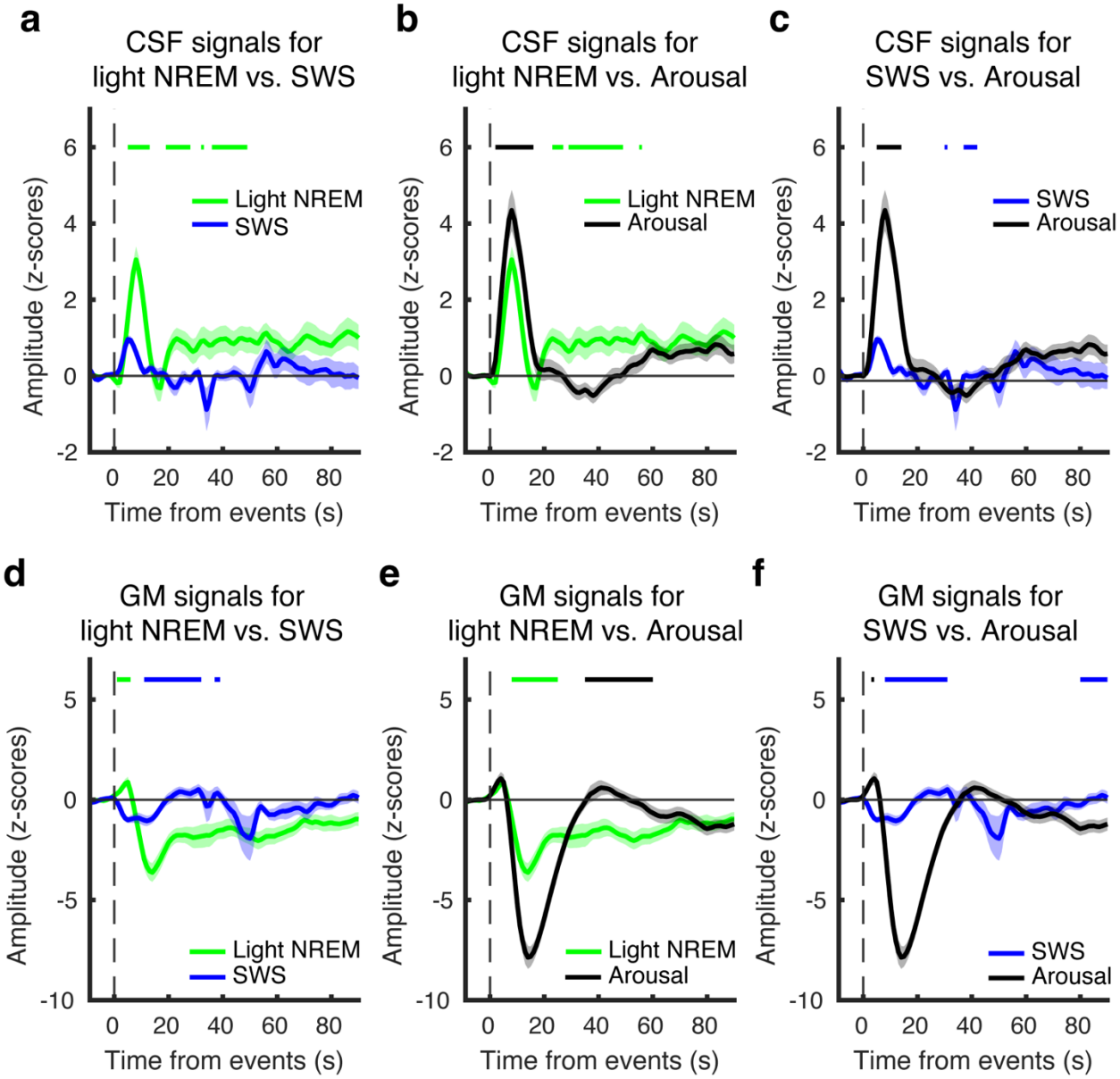

Supplementary Fig. S9: Comparisons of CSF and GM signal changes induced by slow waves in different sleep depths and arousals. a–c, CSF signal changes time-locked to slow waves during sleep and arousals. Green, light NREM sleep; blue, slow-wave sleep; black, arousals. **d–f**, GM signal changes time-locked to slow waves during sleep and arousals. Green, light NREM sleep, blue, slow-wave sleep, black, arousals. The horizontal bars (green: light

1291 NREM; blue, slow-wave sleep; black: arousals) indicate significant differences between possible

1292 pairs using two-tailed paired *t*-tests, (FDR corrected, $Ps < 0.05$). SWS, slow-wave sleep.

1293

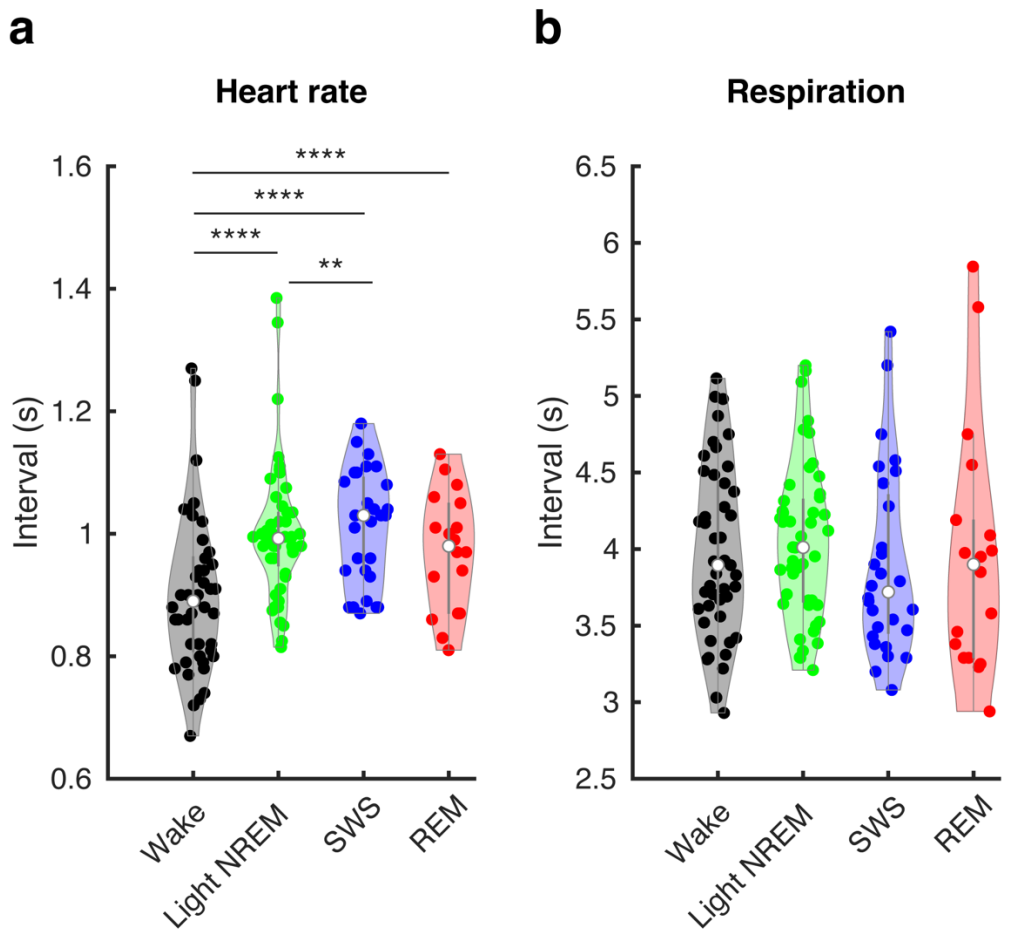

Supplementary Fig. S10: Intervals of cardiac and respiratory cycles during sleep and wakefulness. a, Intervals of cardiac cycles. The intervals of the cardiac cycles were significantly longer during sleep than during wakefulness (light NREM sleep vs. wakefulness: P = 6.80e-12; Slow-wave sleep vs. wakefulness: P = 7.85e-07; REM sleep vs. wakefulness: P = 5.31e-04). Slow-wave sleep had significantly longer intervals than light NREM (P = 0.0011). Two-tailed paired t-tests with Bonferroni correction, ****P<.001, **P<.01. **b**, Intervals of respiratory cycles. There was no significant difference in the intervals of respiratory cycles across sleep stages. SWS, slow-wave sleep.

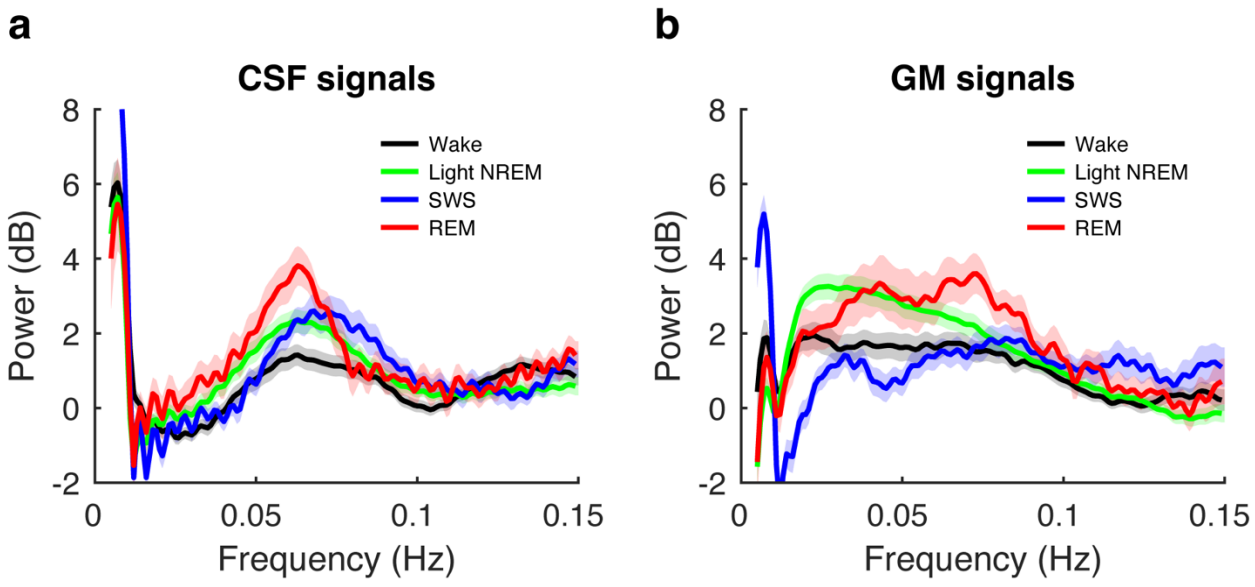

Supplementary Fig. S11: Periodic frequency profiles obtained from the CSF (a) and GM (b) signals without denoising cardiac and respiration signal contaminations.

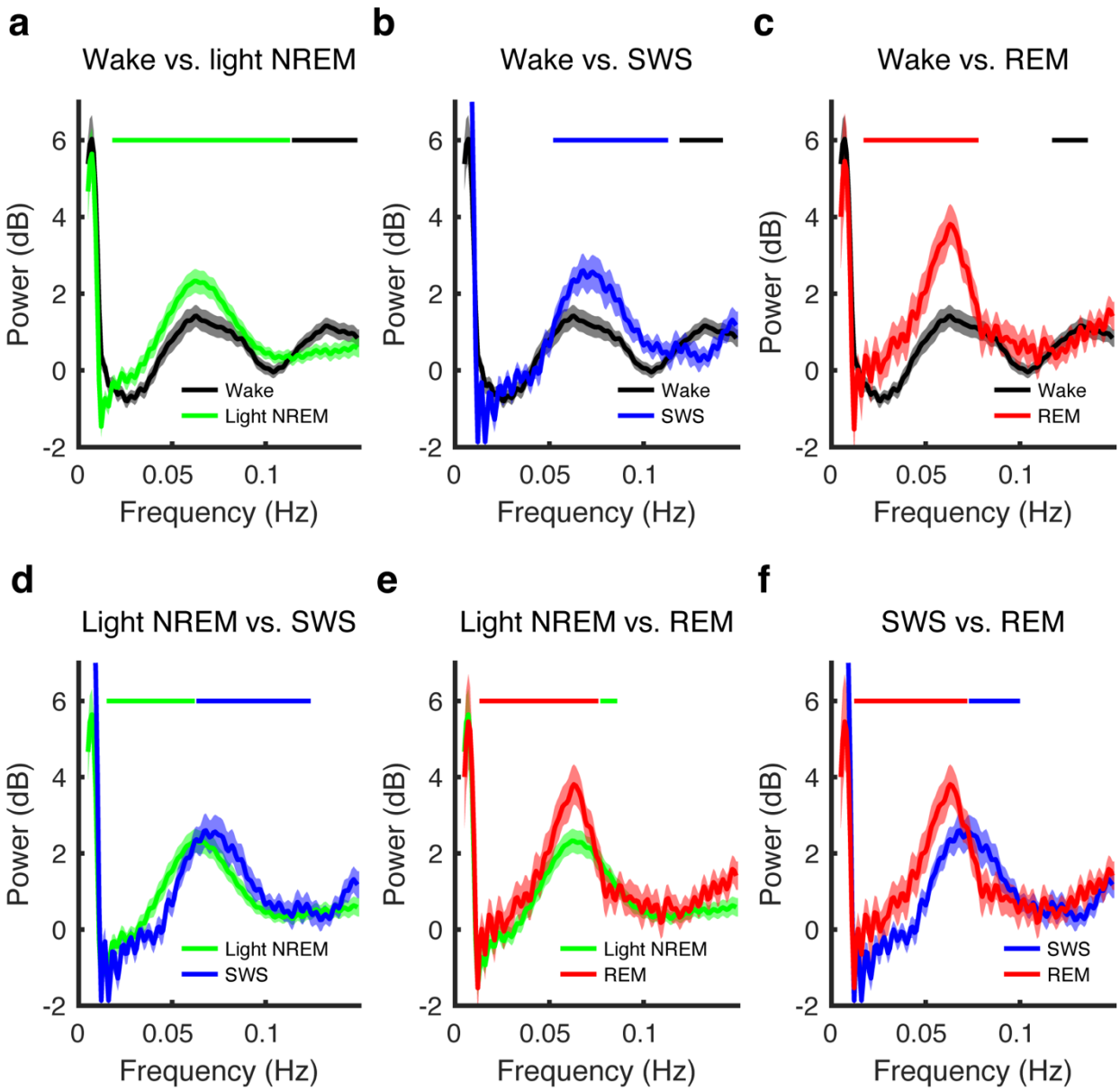

Supplementary Fig. S12: CSF signals without denoising cardiac and respiration signal contaminations. Comparisons of the spectrum against each frequency bin across different sleep depths. **a**, Wakefulness vs. light NREM sleep. **b**, Wakefulness vs. slow-wave sleep. **c**, Wakefulness vs. REM sleep. **d**, Light NREM sleep vs. slow-wave sleep. **e**, Light NREM sleep vs. REM sleep. **f**, Slow-wave sleep vs. REM sleep. Cluster-based permutation results for possible

1318 pairs were conducted. The horizontal bars represent a significant cluster (horizontal bars, cluster-

1319 based permutation tests, *Ps* < 0.05). SWS, slow-wave sleep.

1320

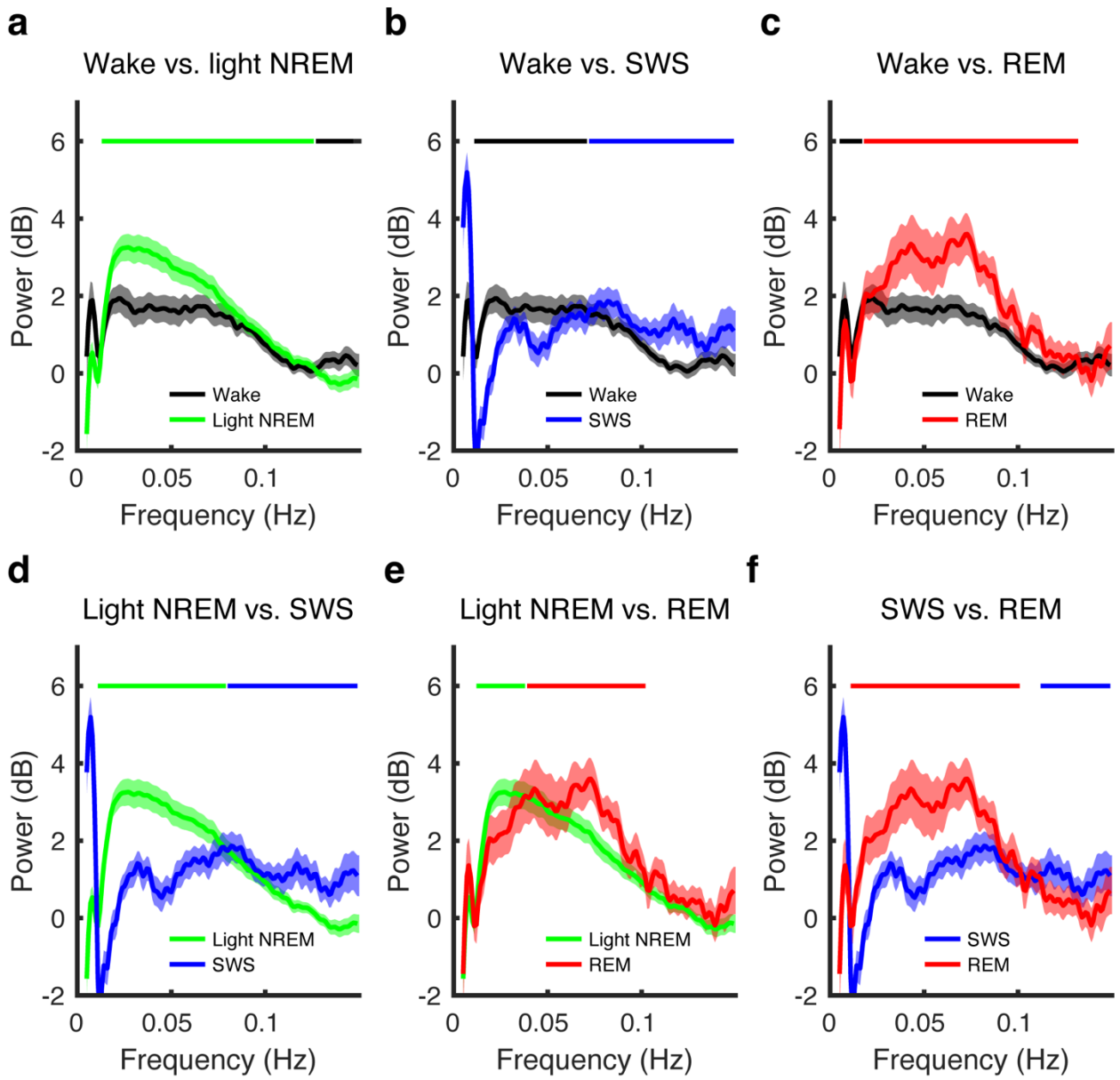

Supplementary Fig. S13: GM signals without denoising cardiac and respiration signal contaminations. Comparisons of the spectrum against each frequency bin across different sleep depths. **a**, Wakefulness vs. light NREM sleep. **b**, Wakefulness vs. slow-wave sleep. **c**, Wakefulness vs. REM sleep. **d**, Light NREM sleep vs. slow-wave sleep. **e**, Light NREM sleep vs. REM sleep. **f**, Slow-wave sleep vs. REM sleep. Cluster-based permutation results for possible

1328 pairs were conducted. The horizontal bars represent a significant cluster (horizontal bars, cluster-

1329 based permutation tests, *Ps* < 0.05). SWS, slow-wave sleep.

1330

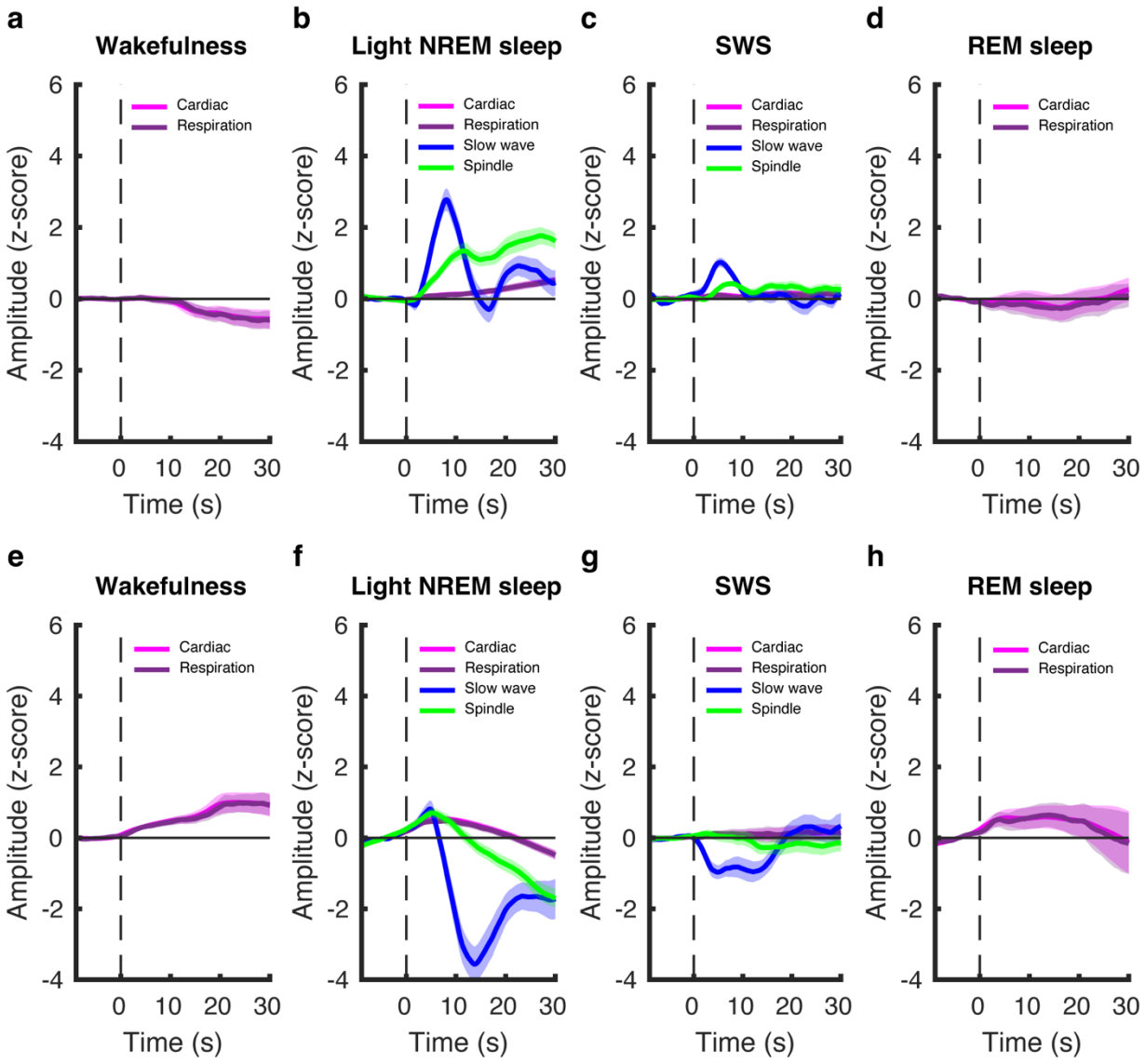

Supplementary Fig. S14: Comparisons of CSF and GM signal changes induced by cardiac pulses and respirations vs. slow waves and sleep spindles in different sleep depths. We investigated the CSF signal changes time-locked to respiration and cardiac pulses in the same manner as in previous studies (Picchioni et al., 2022; Williams et al., 2023). **a–d**, CSF signal changes time-locked to each event onset during each sleep stage. **e–h**, GM signal changes time-

1338 locked to each event onset during each sleep stage. Magenta, cardiac pulses. Purple, respirations,

1339 Blue, slow waves, Green, spindles. SWS, slow-wave sleep.

1340

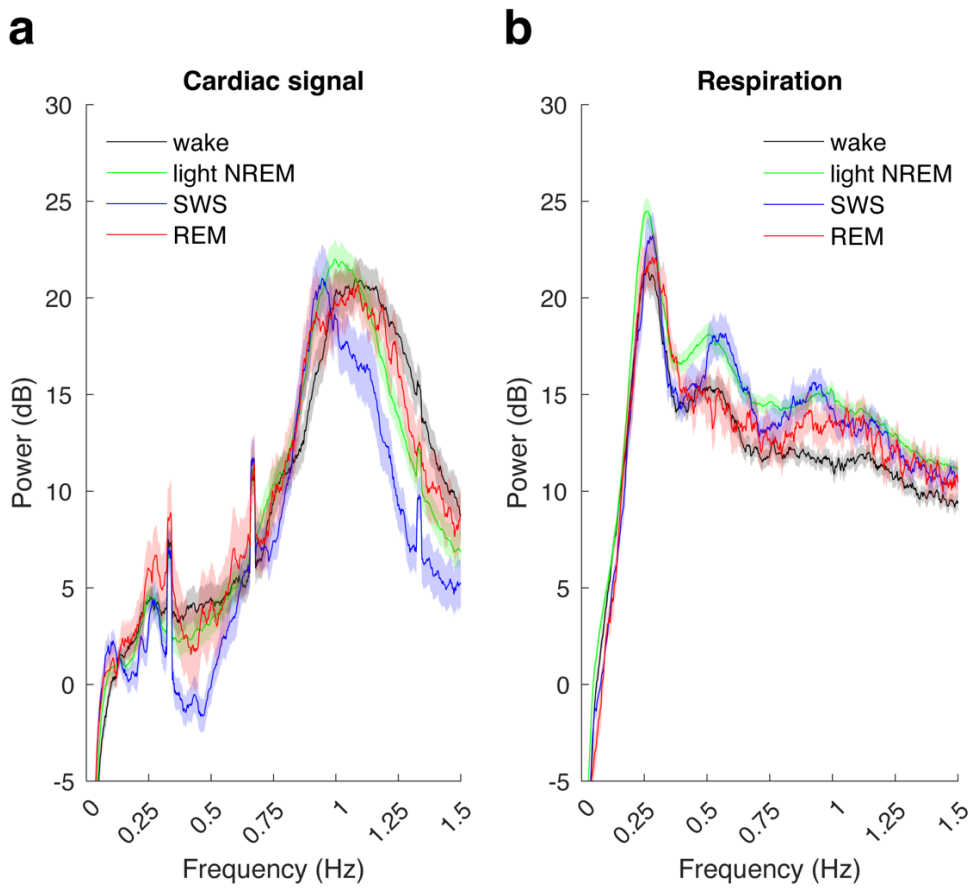

Supplementary Fig. S15: Periodic frequency profiles in the cardiac cycles (a) and the respiration cycles (b). The power spectrum of the cardiac and respiration signals were measured using the same analysis steps as the power spectrum analysis of fMRI data. There was a peak power at around 1 Hz in the cardiac signals, whereas a peak power of around 0.3 Hz was observed in the respiration signals in accordance with a previous study (Strik et al., 2002). Thus, the cardiac and respirations had much higher frequency signals (>0.3Hz) that did not overlap with the frequency range induced by sleep brain oscillations (0.06–0.15Hz, **Fig. 1d, e**).

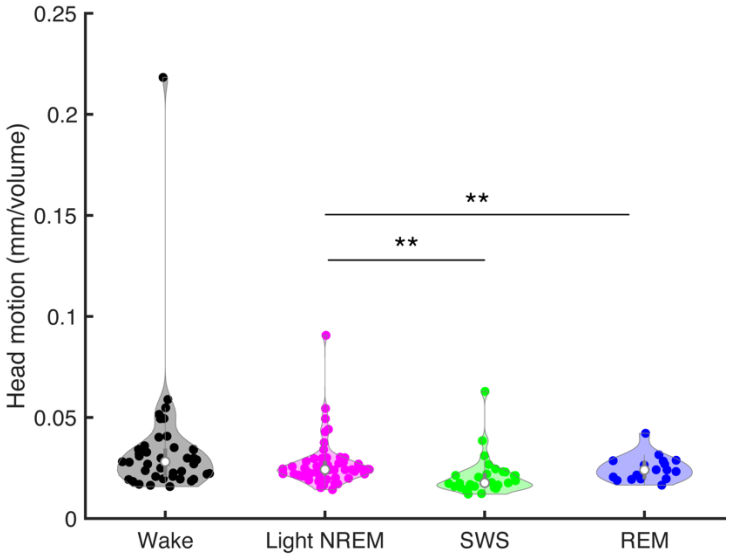

Supplementary Fig. S16: Head motion across different sleep depths. Two-tailed paired *t*-tests with Bonferroni correction, $^{**}P < 0.01$. SWS, slow-wave sleep.